BILINGUAL PUBLISHING CO.
Pioneer of Global Academics Since 1984

Electrical Science & Engineering

Volume 4 • Issue 1 • April 2022 ISSN 2661-3247(Online)

BILINGUAL
PUBLISHING CO.
Pioneer of Global Academics Since 1984

Editor-in-Chief

Editorial Board Members

Volume 4 Issue1 • April 2022 • ISSN 2661-3247 (Online)

Electrical Science & Engineering

BILINGUAL PUBLISHING CO.
Pioneer of Global Academics Since 1984

BILINGUAL PUBLISHING CO.
Pioneer of Global Academics Since 1984

Volume 4 | Issue 1 | April 2022 | Page1-40
Electrical Science & Engineering

Contents

Articles

BILINGUAL PUBLISHING CO.
Pioneer of Global Academics Since 1984

Electrical Science & Engineering
https://ojs.bilpublishing.com/index.php/ese

ARTICLE

Classification and Detection of Amharic Language Fake News on Social Media Using Machine Learning Approach

Kedir Lemma Arega*

School of Technology and Informatics, Department of Information Technology, Ambo University, Ethiopia

ARTICLE INFO

Article history
Received: 16 November 2021
Revised: 31 December 2021
Accepted: 13 January 2022
Published Online: 26 January 2022

Keywords:
Amharic fake news detection
Amharic posts and comments datasets
Classification
Machine learning
Social media

ABSTRACT

The pervasive idea of web-based media stages brought about a lot of sight and sound information in interpersonal organizations. The transparency and unlimited way of sharing the data via online media stage encourages data spread across the organization paying little mind to its noteworthiness. The multiplication of misdirecting data in regular access news sources, for example, web-based media channels, news websites, and online papers has made it trying to recognize dependable news sources, in this way expanding the requirement for computational devices to give bits of knowledge into the unwavering quality of online substance. The broad spread of phony news contrarily affects people and society. Along these lines, counterfeit news identification via web-based media has as of late become arising research drawing in enormous consideration. Observing the possible damage caused by the rapid spread of fake news in various fields such as politics and finance, the use of language analysis to automatically identify fake news has attracted the attention of the research community. A social networking service is a platform for people with similar interests, activities, or backgrounds to form social networks or social relations. Participants who register on this site with its own expression (often a profile) and social links are generally offered a social network service.

1. Introduction

Counterfeit news is anything but an original idea. Strikingly, the thought has been in presence even before the development of the Web as distributers utilized bogus and deceiving data to additional their advantages [1]. The most serious issue of these days' online media papers is generally phony news stories [2]. There is an increment in the dispersion of bogus news, tricks and other misleading statements in the public eye. The distribution of phony information is going not just on a virtual world (web-based media, social network, and so forth) yet additionally from one individual to another. Counterfeit news is a major string since it can influence many individuals all throughout the planet consistently [3]. Counterfeit news is progressively turning into a threat to our general public.

*Corresponding Author:
Kedir Lemma Arega,
School of Technology and Informatics, Department of Information Technology, Ambo University, Ethiopia;
Email: kedirnaw1999@gmail.com

DOI: https://doi.org/10.30564/ese.v4i1.3885

It is normally produced for business interests to draw in watchers and gather promoting income. Notwithstanding, individuals and gatherings with conceivably pernicious plans have been known to start counterfeit news to impact occasions and approaches around the world. The use of the Internet has grown in recent years. The term "social media networks" has gained popularity as a result of the widespread use of the Internet. Everyone who uses the Internet is familiar with online access [4]. An online access is a grouping of several social networking websites. Online network is a platform that allows users to express their opinions about anything [5].

Online Social Networks are the most popular way for people all over the world to exchange information. Social networks are the focal point people use these devices for many different purposes and they provide a variety of new tools for the user community. A social network is best described as a graphical structure with nodes and edges representing users and their interactions [6]. Depending on the network structure used, the nodes and edges in a Social Network graph can be labelled or unlabelled. Because of social intelligence's high reputation, social networking sites such as Facebook, WhatsApp, Twitter, Instagram and Telegram has become the tool of choice for communicating and sharing information with a wide variety of users, including individuals and businesses [7]. Customers of online media will play an important role and will be solely responsible for the information exchanged on the networks. Users share information from websites, videos, and files that they find interesting. People share confidential information with great faith, and others have the same faith in the information shared. The surge in the reputation of online social networks, as well as the availability of a massive amount of data, allows them to be simple targets for their opponents. These goals primarily include stealing personal information from individual users without their knowledge [7].

1.1 Definition of Fake News

Counterfeit news definition is made of two sections: validness and plan. Genuineness implies that phony news content bogus data can be confirmed all things considered, which implies that paranoid fear is excluded from counterfeit information as there are hard to be refuted valid or as a rule [8]. The subsequent part, purpose, implies that the bogus data have been composed to misdirect the peruse.

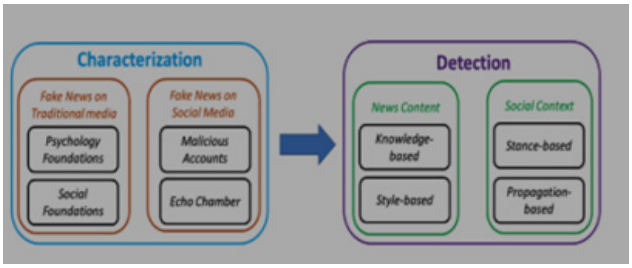

Figure 1. Fake news on social network: characterization to detection flow diagram [6]

1.2 The Amharic Linguistic

"Amharic is an Ethiopian Semitic language, which is a subgrouping inside the Semitic part of the Afroasiatic dialects. It is communicated in as a first language by the Amharas, and furthermore fills in as a most widely used language for different populaces living in significant urban areas and towns of Ethiopia

1.2.1 The Representation of Amharic Characters

Geez characters, which date back to the 4th century AD, are used in Amharic. The original Geez writing forms contained only consonants, while subsequent variants of the symbols represented consonant-vowel phoneme pairs. Amharic writing, like Geez, uses a combination of vowels and consonants. The Amharic language uses seven vowels, each in seven different forms, which correspond to seven vowel sounds. There are 33 basic characters, each of which represents a consonant and a vowel at the same time, making the Amharic script pronounced in syllables [11].

1.2.2 Punctuation Marks of Amharic Language

Recognizing accentuation marks is crucial to know word boundary for regular language handling. As indicated by Tewodros Hailemeskel (2003), the accentuation marks in Amharic are around ten however not many of them utilized in the PC composing framework. "HuletNeteb" (":") word separator and "AratNeteb" ("::") sentence separator are the significant accentuation marks. However, space is generally utilized rather than HuletNeteb (":"), especially in PC composing [5].

1.2.3 Amharic Number

Bender et al. (1976) expressed that Amharic numbers are gotten from Greek letters. Furthermore, some of them were adjusted to seem as though Amharic person [1]. They are addressed by a solitary letter, and every one of them has a level stroke above and underneath, as displayed in the accompanying table [16].

Table 1. Amharic Number System

፩	፪	፫	፬	፭	፮	፯	፰	፱	፲	፳	፴	፵	፶	፷	፸	፹	፺	፻
1	2	3	4	5	6	7	8	9	10	20	30	40	50	60	70	80	90	100	1000

1.3 Difficulties in the Amharic Penmanship Scheme

The Amharic writing plan includes a few difficulties that are difficult to cope with while dealing with Amharic text. One of these challenges is the repeating of characters in Amharic, which requires more than one person to address 19 the same sound. In Ge'ez, the various structures are significant, but in Amharic, there is no unambiguous concept that explains why they exist [5]. The issue of the same sound with different characters is evident with the central characters, as well as in similar character requests. Those are, ሀ and ሃ; ሐ and ሓ; ኻ and ኽ; አ and ኣ A word that is framed using this person has a comparable meaning.

Table 2. Amharic Penmanship Scheme Sound

Character	The other style of character	Others
ሀ (he)	ሐ and ኻ	ሃ ፡ ሓ ፧ ኽ
ሠ (se)	ሰ	
አ (a)	ዐ	ኣ ፧ ዓ
ጸ (tse)	ፀ	

2. Literature Review

A broad writing audit would be directed on programmed counterfeit news identification, language innovation, and Amharic language to know the topic exhaustively. In this paper, multiple researches were provided with diverse ways to detect false news, and they proposed a classification system for detecting fake news on social media. Following Table 3 shows works done by

Table 3. Summary of related work

Researcher	Topics	Extract feature	Accuracy and result
WorkuKelemework(2013)	Automatic Amharic text news classification: a neural networks approach	Automatic classification of Amharic news using neural network method	In order to compare the effectiveness of the Vector Quantization (VQ) algorithm, a TF*IDF weighting method was used. The accuracy for this experiment was an average of 71.96%.
Nicole O'Brien (2018)	Machine Learning for Detection of Fake News	Machine learning	95.8 %.
Samir Bajaj (2017)	Fake News Detection Using Deep Learning	Using Deep Learning	0.7
Yi-Ju Lu, Cheng-Te Li (2020)	Graph-aware Co-Attention Networks for Explainable Fake News Detection on Social Media	Using GCAN	16%
Md ZobaerHossainy|, Md Ashraful Rahmany|, Md Saiful Islam|, Sudipta Kar (2020)	BanFakeNews: A Dataset for Detecting Fake News in Bangla	Using traditional Linguistic features and neural network-based methods.	90%
Ajeet Ram Pathaka, Aditee Mahajana, Keshav Singha, Aishwarya Patila, Anusha Naira (2019)	Analysis of Techniques for Rumour Detection in Social Media	Use comparative analysis of the state-of-the-art	Accuracy 82%
Josef Kapusta, Petr Hajek, Michal Munk, Lubomir Benko (2020)	Comparison of fake and real news based on morphological analysis	Using morphological analysis	to improve the existing web services for fake news classification
MontherAldwairi, Ali Alwahedi (2018)	Detecting Fake News in Social Media Networks	Use both Bayes Net and Naïve Bayes	94.4%

different researchers on these topics [2,3,7,8,12,13].

3. Methodologies

The algorithms we create to classify bogus news written in Amharic are described in this section. Traditional lang uage features as well as several neural network-based models are used in our method.

3.1 Dataset Construction

The goal of this research is to identify Amharic bogus news on social media. In addition, a new Amharic false news dataset must be created.

3.2 Traditional Linguistic Features

3.2.1 Lexical Characteristics

We extract word n-grams (n=1, 2, 3) and character n-grams (n=3, 4, 5) from news articles due to strong performance in several text categorization tasks. We use the phrase frequency-inverse document frequency as a weighting system (TFIDF).

3.2.2 Grammatical Structures

The Grammatical features of texts are frequently important for deciphering specific examples in reports that assist order issues in the end.

3.2.3 Semantic Features

By providing semantic data, dispersed depictions of word and sub-word tokens have demonstrated adequacy in text order difficulties. As a result, we experiment with several approaches to pre-prepared word inserting, such as addressing an article based on the mean and standard deviation of the vector representations of the words in it.

3.3 Punctuation and Metadata

We noticed a higher presence of some accentuation images like "!" in the phony news. Thusly, we utilize the accentuation recurrence as provisions. Moreover, we utilize some Meta data like the lengths of the feature and

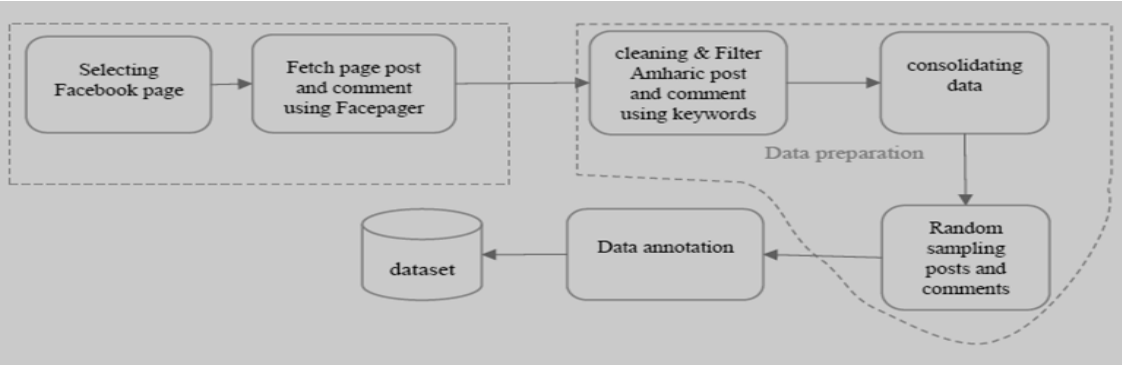

Figure 2. Technics for Building Amharic Fake News Dataset

Table 4. Some Category of Social Media Page

S.No.	Name of Category	Description for the Name
1	News media and Broadcasting pages	Conveying the news to the overall population or an objective public
2	Bloggers and Journalists pages	An individual who consistently composes material for a blog. Likewise, an individual composes for papers, magazines, or news sites or plans news to communicate.
3	Religious Group Pages and Media	Conveying strict news, strict lessons to the devotees of that religion or an objective gathering.
4	Official Pages of Political Parties, Politicians, and Government Offices	Gathering of individuals, frequently lawmakers with normal perspectives, meet up to challenge decisions and capture the power in the public authority. A gathering of legislators who have held the force of government
5	Public figure Artist and Authors pages	An individual or person of note who makes tune, painting or an essayist of a book, article, or archive.
6	Community Pages for Activists, General, or Special Interests	An individual who missions to achieve political or social change: additionally, pages advance diverse political, strict.

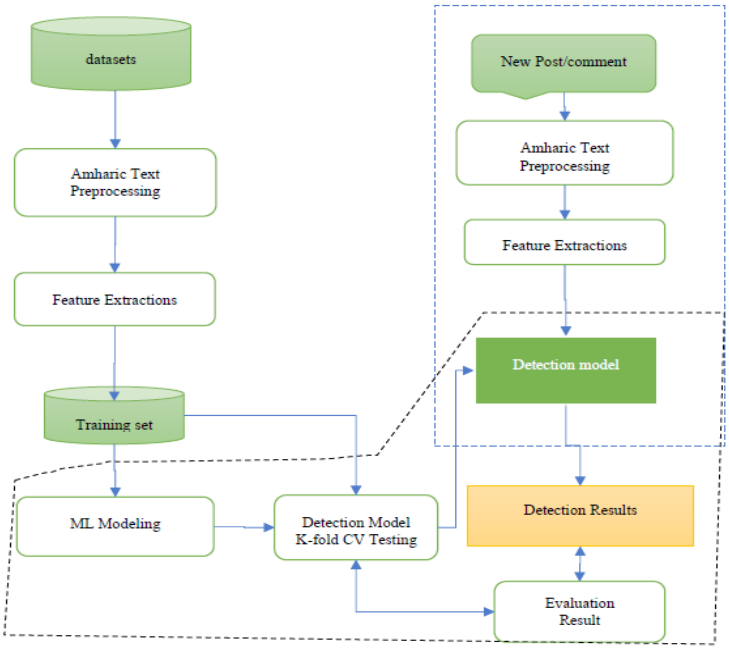

Figure 3. Amharic Fake News Detection Architecture

the assortment of news stories as provisions.

3.4 Neural Network Models

Neural organizations are exhibiting amazing execution in a wide scope of text characterization and age errands. Given a lot of preparing information, such models normally accomplish higher precision than etymological element based strategies. Consequently, we try different things with a few neural organization models that have been utilized as benchmark models in various text order errands.

3.5 Evaluation Metrics

To assess each model, different assessment measurements have been utilized. There are review, accuracy and f1-score. It is expected to utilize various measurements since they don't all record for similar qualities. For example, it is feasible to have a model with a review of 1 that act very terrible on the grounds that it just groups every one of the contributions to a similar single class.

Remind it Precision is expressed as [6].

$$Precision = \frac{TP}{TP + FP}$$

This indicates that depending on which classes are considered positive, we can have two distinct precisions. It is a ratio of appropriately categorized optimistic features to the total number of positive elements. When there are no false positives, it equals 1, but this does not mean that all of the positive elements have been correctly identified; there could be some erroneous negatives. The recall aids in the resolution of this issue.

It is express as

$$Recall = \frac{TP}{TP + FN}$$

The f1-score combines the recall and the precision. It is defined by

$$f1 - score = \frac{2 * precision * recall}{precision + recall}$$

You can likewise check out the weighted normal of these numbers. For instance, the worldwide review can be determined by duplicating the review for the two classes by the applicable class proportion [12].

4. Proposed System

A tool that can identify and delete fraudulent sites from the results presented to a user by a search engine or a social media news feed is part of the proposed system to address the issue of false news. The user can download the tool and then add it to the browser or program they use to get news feeds. Once it's up and running, the tool will use a variety of techniques, including those that look at a link's syntactic features, to determine whether it should be included in the search results [8].

5. Conclusions

Privacy concerns and the disclosure of private data

consume emerged as the greatest pressing concerns for social networking services. Users from all across the world use social networking services in various ways. The simplicity with which fake users and other dangerous users can contact these people and use the information stored in their accounts attracts them. This article proposed to foster an answer for counterfeit news via web-based media utilizing AI methods. The review attempted to create, execute and thinks about AI and text highlight extraction techniques explicitly for counterfeit news recognition for the Amharic language. The point further developed the current online media administrations for counterfeit news characterization.

References

[1] Fikremariam, Genet Mezemir, 2009. Automatic Stemming for Amharic Text: An Experiment Using Successor Variety Approach. pp. 1-79.

[2] Kelemework, Worku, 2013. Automatic Amharic text news classification: Aneural networks approach. Ethiop. J. Sci. & Technol. Vol. 6, pp. 127-137.

[3] Bajaj, Samir, 2017. Fake News Detection Using Deep Learning. Stanford University: cs 224n.

[4] Srinivas Rao Pulluri, Jayadev Gyani, Narsimha Gugulothu, 2017. A Comprehensive Model for Detecting Fake Profiles in Online Social Networks. International Journal of Advanced Research in Science and Engineering. Vol. 6, pp. 1-10.

[5] Ver´onica P´erez-Rosas, Bennett Kleinberg, Alexandra Lefevre, August 20-26, 2018. Automatic Detection of Fake News. Santa Fe, New Mexico, USA. s.n. 2018. Proceedings of the 27th International Conference on Computational Linguistics. pp. 3391-3401.

[7] Lorent, Simon. 2018-2019. Fake News Detection Using Machine. pp. 1-91.

[8] O'Brien, Nicole, 2018. Machine Learning for Detection of Fake News. pp. 1-56.

[9] Ajeet Ram Pathaka, Aditee Mahajana, Keshav Singha, Aishwarya Patila, Anusha Naira, 2019. Analysis of Techniques for Rumor Detection in Social Media. International Conference on Computational Intelligence and Data Science (ICCIDS 2019). pp. 1-11.

[10] Sachin Ingle, Satish Borade, Sagar Awasare, 2019. Detecting Fake User Accounts on. IJARIIE-ISSN(O)-2395-4396. pp. 927-931.

[11] Defar, Yonas Kenenisa. 2019. Hate Speech Detection for Amharic Language on Social Media Using Machine Learning Techniques. pp. 1-103.

[12] Lu, Y.J., Li, Ch.T., 2020. GCAN: Graph-aware Co-Attention Networks. arXiv, Vol. 1, pp. 1-10.

[13] Md Zobaer Hossainy, Md Ashraful Rahmany, Md Saiful Islam, Sudipta Kar. Bangla, BanFakeNews: A Dataset for Detecting Fake News in. 2020, University of Houston, Texas, USA. pp. 1-10.

[14] Arega, Kedir Lemma, 6, 2020. Social Media Fake Account Detection for Amharic Language. Global Scientific Journals. Vol. 8, pp. 604-614.

[15] Josef Kapusta, Petr Hajek, Michal Munk, Lubomir Benko, 2020. Comparison of fake and real news based on morphological analysis. ELSEVIER. pp. 1-9.

[16] Kai Shuy, Amy Slivaz, Suhang Wangy, Jiliang Tang, Huan Liuy. Fake News Detection on Social Media:A Data Mining Perspective.

BILINGUAL PUBLISHING CO.
Pioneer of Global Academics Since 1984

Electrical Science & Engineering
https://ojs.bilpublishing.com/index.php/ese

ARTICLE

Research on Self-balancing Two Wheels Mobile Robot Control System Analysis

Hla Myo Tun[1*] Myat Su Nwe[2] Zaw Min Naing[3] Maung Maung Latt[4] Devasis Pradhan[5] Prasanna Kumar Sahu[6]

1. Faculty of Electrical and Computer Engineering, Yangon Technological University, Yangon, Myanmar
2. Department of Mechanical Engineering, King Lauk Phya Institute of Technology Myaungmya, Myaungmya, Myanmar
3. Department of Research and Innovation, Ministry of Science and Technology, Yangon, Myanmar
4. Department of Electronic Engineering, Yangon Technological University, Yangon, Myanmar
5. Department of Electronics & Communication Engineering, Acharya Institute of Technology, Bengaluru, India
6. Department of Electrical Engineering, National Institute of Technology, Rourkela, Odisha, India

ARTICLE INFO

Article history
Received: 24 January 2022
Revised: 17 March 2022
Accepted: 28 March 2022
Published Online: 13 April 2022

Keywords:
Mobile robot
Self-balancing robot
Control system design
PID controller
Dynamic control system analysis

ABSTRACT

The paper presents the research on self-balancing two-wheels mobile robot control system analysis with experimental studies. The research problem in this work is to stabilize the mobile robot with self-control and to carry the sensitive things without failing in a long span period. The main objective of this study is to focus on the mathematical modelling of mobile robot from laboratory scale to real world applications. The numerical expression with mathematical modelling is very important to control the mobile robot system with linearization. The fundamental concepts of dynamic system stability were utilized for maintaining the stability of the constructed mobile robot system. The controller design is also important for checking the stability and the appropriate controller design is proportional, integral, and derivative – PID controller and Linear Quadratic Regulator (LQR). The steady state error could be reduced by using such kind of PID controller. The simulation of numerical expression on mathematical modeling was conducted in MATLAB environments. The confirmation results from the simulation techniques were applied to construct the hardware design of mobile robot system for practical study. The results from simulation approaches and experimental approaches are matched in various kinds of analyses. The constructed mobile robot system was designed and analyzed in the control system design laboratory of Yangon Technological University (YTU).

*Corresponding Author:
Hla Myo Tun,
Faculty of Electrical and Computer Engineering, Yangon Technological University, Yangon, Myanmar;
Email: hlamyotun@ytu.edu.mm

DOI: https: //doi.org/10.30564/ese.v4i1.4398

1. Introduction

Mobile robots are empowered for military and industries and became popular in helping domestic works like a four-wheel vacuum cleaner and hospitals like a motorised wheelchair, among those various robots such as a four-wheel robot, dog robot, spider robot, etc. [1,2]. The two-wheel self-balancing robot invented by Segway is one of the innovative robot solutions from personal robotics applications to private transportation. The idea of developing Segway personal transport, which can balance on its two wheels, has drawn interest from many researchers worldwide. Such kind of robot can solve several challenges in industry and society [3-5]. Because being a small and light cart allows humans to travel in small areas or factories where cars cannot enter with less pollution and less power consumption. Moreover, a Segway robot is interesting because it combines sensory capability and intelligent control methods to keep the robot in equilibrium [6-8].

The two-wheeled self-balancing robot is similar to the configuration of Segway based on inverted pendulum theory. The increasing affordability of commercial off-the-shelf (COTS) sensing components and microprocessor boards has become one of the key reasons to widely research and report. The two-wheeled self-balancing robot is a kind of robot that can balance itself on two wheels [9-11]. This robot chassis was designed in the SolidWorks software and fabricated with a laser cutter using acrylic materials. Then it was mounted on two 12 V DC motors 500 rpm with the encoder. In this project, an inertial measurement unit (IMU) called MPU6050, consisting of 3 axis accelerometer and a three-axis gyroscope, was chosen to measure the robot orientation (roll, pitch, and yaw). It consists of some weak points in the gyroscope and accelerometer when they are used alone [12].

Consequently, the data received from IMU were converted to the tilt angle and passed through one of the filters. A complimentary filter is used for data fusion to get the perfect angle. To balance the device, a controller plays an essential role in the self-balancing robot. PID controller is used in this project to control the speed of the motor via the PWM duty cycle. The robot's power can be given by using a battery placed on top of the chassis [13]. In this way, the aim of balancing the robot was fully achieved.

Because of higher speed due to less friction from fewer wheels, more straightforward structural design, lesser parts that need replacing over time, such as wheels, this two-wheeled self-balancing robot can be used in various applications with different perspectives such as an intelligent gardener in agricultural fields, an autonomous trolley in hospitals, shopping malls, offices, airports, healthcare applications or an intelligent robot to guide blind or disable people [14]. The general objectives to perform this research are to design and fabricate a relevant balancing two-wheeled robot chassis, to derive the mathematical model [15] of the system, to illustrate the schemes and techniques involved in balancing unstable robotic environments on two wheels using proper motors, sensors and a suitable microprocessor, and to design a complete stable discrete digital control system in the appropriate software.

In this work, we emphasized the derivation of a mathematical model based on the inverted pendulum theory, design of two-wheeled robot in SolidWorks software, implementation of the filter for IMU sensor and PID control, integration of the robot's controller with hardware, and testing, analysing and troubleshooting for the whole system. The authors have solved the stabilizing problem for the mobile robot with self-control and to carry the sensitive things without failing in a long span period. The detailed analyses and numerical expression on mathematical modellings were discussed in the following section. The research motivation on the mobile robot system implementation is how to link the simulation approaches to experimental approaches in real time applications.

The paper is organised as follows. Section II presents the dynamic mathematical model of the targeted mobile robot. Section III mentions the control system design. Section IV points out the hardware implementation. Section V gives the results and discussions on the theoretical and experimental studies. The last section is the conclusion of the research work.

2. Mathematical Modelling

The mathematical modelling for the self-balancing mobile robot system could be completed based on the respective section on the dynamical system appraoches. The first portion is concerning the linear model of a DC motor for that mobile robot and the second portion is the dynamic model of mobile robot.

2.1 Linear Model of a Direct Current (DC) Motor

Two 500 rpm DC motors are used to power the robot. In this section, the state-space model of the DC motor, which is necessary for deriving the balancing robot's dynamic model, is expressed. Consequently, the relationship between the input voltage to the motors and the control torque required to stabilise the robot is obtained.

Figure 1 expresses an effective linear model for a direct current motor. When a voltage is applied to the dc motor, a current (i) is generated. As a result, a motor torque, which is proportional to the current, is produced. The equation can be expressed as

$$\tau_m = k_m \times i \tag{1}$$

An electromotive force (emf) is induced when the coil of a motor is spinning through a magnetic field due to an applied voltage source. In other words, the motor's shaft is turning, and emf is generated when the motor is in an operation mode. Thus, back emf voltage increases proportionally to the shaft velocity w, which can be written as

$$V_{en} = k_e \times \omega \tag{2}$$

By using Kirchoff's Voltage Law, the linear differential equation of the DC motor's electrical circuit can be written as

$$-V_s + i \times R + L \times \frac{di}{dt} + V_{en} = 0 \tag{3}$$

$$\frac{di}{dt} = \frac{V_s}{L} - \frac{iR}{L} - \frac{V_{en}}{L} \tag{4}$$

$$\frac{di}{dt} = -\frac{R}{L} \times i - \frac{k_e}{L} \times \omega + \frac{V_s}{L} \tag{5}$$

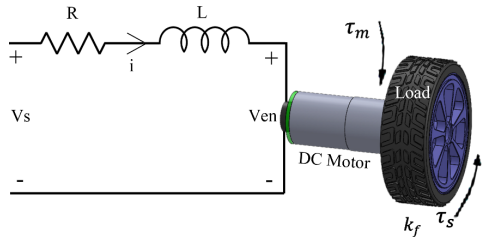

Figure 1. Diagram of a DC motor

According to Newton's Law of Motion, the summation of all torques produced on the shaft is linearly related to the acceleration of the shaft by the inertial load of the armature. The motion equation can be written

$$\sum M = I_R \times \alpha \tag{6}$$

$$\sum M = I_R \times \dot{\omega} \tag{7}$$

$$\tau_m - k_f \omega - \tau_s = I_R \dot{\omega} \tag{8}$$

$$k_m i - k_f \omega - \tau_s = I_R \frac{d\omega}{dt} \tag{9}$$

$$\frac{d\omega}{dt} = \frac{k_m}{I_R} i - \frac{k_f}{I_R} \omega - \frac{1}{I_R} \tau_s \tag{10}$$

Assume that the motor's inductance (L) and motor's friction (k_f) is approximately zero. Equation (3) and Equation (10) become Equation (12) and Equation (13), respectively.

$$-V_s + iR + V_e = 0 \tag{11}$$

$$i = -\frac{k_e}{R} \omega + \frac{1}{R} V_s \tag{12}$$

$$\frac{d\omega}{dt} = \frac{k_m}{I_R} i - \frac{1}{I_R} \tau_s \tag{13}$$

By substituting Equation (12) into Equation (13), an approximation for the DC motor, which is only a function of the current motor speed (ω), applied voltage (V_s) and applied torque (τ_s) is obtained.

$$\frac{d\omega}{dt} = \frac{k_m}{I_R} \left(-\frac{k_e}{R} \omega + \frac{1}{R} V_s \right) - \frac{1}{I_R} \tau_s \tag{14}$$

$$\frac{d\omega}{dt} = -\frac{k_m k_e}{I_R R} \omega + \frac{k_m}{I_R R} V_s - \frac{1}{I_R} \tau_s \tag{15}$$

A state-space model can represent the dynamic model of the motor. This state-space consists of two state variables: angle (θ) and velocity (ω). The input variables for the motor is the applied voltage (V_s) and applied torque (τ_s).

$$\begin{bmatrix} \dot{\theta} \\ \dot{\omega} \end{bmatrix} = \begin{bmatrix} 0 & 1 \\ 0 & -\frac{k_m k_e}{I_R R} \end{bmatrix} \begin{bmatrix} \theta \\ \omega \end{bmatrix} + \begin{bmatrix} 0 & 0 \\ \frac{k_m}{I_R R} & -\frac{1}{I_R} \end{bmatrix} \begin{bmatrix} V_s \\ \tau_s \end{bmatrix} \tag{16}$$

$$y = \begin{bmatrix} 1 & 0 \end{bmatrix} \begin{bmatrix} \theta \\ \omega \end{bmatrix} + \begin{bmatrix} 0 & 0 \end{bmatrix} \begin{bmatrix} V_s \\ \tau_s \end{bmatrix} \tag{17}$$

The outcome of Equation (17) is the estimated mobile robot position in experimental studies.

2.2 Dynamic Modelling of Mobile Robot System

This two-wheeled self-balancing robot is a kind of complex dynamic system because of the nature of an inverted pendulum on a cart. Two equations of motion, which can completely describe the heart of the balancing robot, are driven by analysing the robot's chassis and wheels separately.

The mathematical model will accommodate such forces as disturbances, and the motor's torque can influence the robot's behaviour. First of all, the equation of motion associated with the left and right wheels is obtained. Since the equation for the left and right wheels are absolutely analogous, only the equation for the right wheel is given. Figure 2 expresses the free body diagram for both wheels.

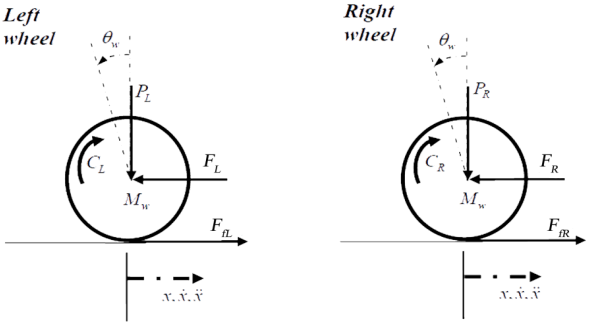

Figure 2. Free body diagram of the wheels

According to Newton's law of motion, the summation of forces on the horizontal x-direction is

$$\sum F_x = Ma \tag{18}$$

$$F_{fR} - F_R = M_w \ddot{x} \tag{19}$$

Adding the moments about the centroid of the wheel gives Equation (20).

$$\sum M_O = I\alpha \tag{20}$$

$$C_R - F_{fR} r = I_w \ddot{\theta}_w \tag{21}$$

The motor torque can be expressed from DC motor dynamics, and the equation can be described as,

$$\tau_m = I_R \frac{d\omega}{dt} + \tau_s \tag{22}$$

By rearranging the equation and substituting Equation (15) into Equation (22), the output torque to the wheels is attained.

$$\tau_m = I_R \left[-\frac{k_m k_e}{I_R R} \dot{\theta}_w + \frac{k_m}{I_R R} V_s - \frac{1}{I_R} \tau_s \right] + \tau_s \tag{23}$$

$$C = -\frac{k_m k_e}{R} \dot{\theta}_w + \frac{k_m}{R} V_s \tag{24}$$

Therefore, Equation (4) becomes

$$-\frac{k_m k_e}{R} \dot{\theta}_w + \frac{k_m}{R} V_s - F_{fR} r = I_w \ddot{\theta}_w \tag{25}$$

Thus,

$$F_{fR} = -\frac{k_m k_e}{Rr} \dot{\theta}_w + \frac{k_m}{Rr} V_s - \frac{I_w}{r} \ddot{\theta}_w \tag{26}$$

The equation of left and right wheels can be obtained by substituting Equation (26) into Equation (19).

For the right wheel,

$$M_w \ddot{x} = -\frac{k_m k_e}{Rr} \dot{\theta}_w + \frac{k_m}{Rr} V_s - \frac{I_w}{r} \ddot{\theta}_w - F_R \tag{27}$$

For the left wheel,

$$M_w \ddot{x} = -\frac{k_m k_e}{Rr} \dot{\theta}_w + \frac{k_m}{Rr} V_s - \frac{I_w}{r} \ddot{\theta}_w - F_L \tag{28}$$

The angular rotation can be converted into linear motion by straightforward transformation because the linear motion is acting on the central point of the wheel.

$$\ddot{\theta}_w r = \ddot{x} \rightarrow \ddot{\theta}_w = \frac{\ddot{x}}{r} \tag{29}$$

$$\dot{\theta}_w r = \dot{x} \rightarrow \dot{\theta}_w = \frac{\dot{x}}{r} \tag{30}$$

By the linear transformation, Equation (27) and Equation (28) becomes:

For the right wheel,

$$M_w \ddot{x} = -\frac{k_m k_e}{Rr^2} \dot{x} + \frac{k_m}{Rr} V_s - \frac{I_w}{r^2} \ddot{x} - F_R \tag{31}$$

For the left wheel,

$$M_w \ddot{x} = -\frac{k_m k_e}{Rr^2} \dot{x} + \frac{k_m}{Rr} V_s - \frac{I_w}{r^2} \ddot{x} - F_L \tag{32}$$

By adding Equation (31) and Equation (32), the first equation of motion for the balancing robot is obtained.

$$2\left[M_w + \frac{I_w}{r^2} \right] \ddot{x} = -\frac{2k_m k_e}{Rr^2} \dot{x} + \frac{2k_m}{Rr} V_s - \left(F_L + F_R \right) \tag{33}$$

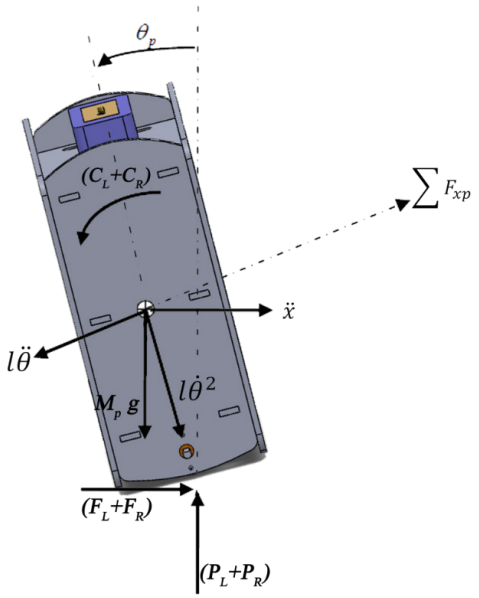

Figure 3. Free Body Diagram of the Chassis

The free body diagram of the chassis is illustrated in Figure 3. In this figure, the Newton's law of motion for self-balancing mobile robot dynamic system based on the mathematical expressions. The mathematical modelling of that free body diagram could be evaluated in the following section.

$$\sum F_P = M_P \ddot{x} \tag{34}$$

$$\left(F_L + F_R \right) - M_p l \ddot{\theta}_p \cos\theta_p + M_p l \dot{\theta}_p^2 \sin\theta_p = M_p \ddot{x} \tag{35}$$

The self-motion could be observed by changing the parameter of "p" for left and right position.

Thus

$$\left(F_L + F_R \right) = M_p l \ddot{\theta}_p \cos\theta_p - M_p l \dot{\theta}_p^2 \sin\theta_p + M_p \ddot{x} \tag{36}$$

Summing the forces perpendicular to the chassis can also give the second equation of motion for the system.

$$\sum F_{xp} = M_p \ddot{x} \cos\theta_p \tag{37}$$

$$\begin{aligned}&\left(F_L+F_R\right)\cos\theta_p+\left(P_L+P_R\right)\sin\theta_p\\&-M_pg\cos\theta_p-M_pl\ddot{\theta}_p=M_p\ddot{x}\cos\theta_p\end{aligned}\tag{38}$$

To get rid of the F and P terms in the above equation, by summing the moments around the centre of mass of chassis, Equation (39) is obtained.

$$\sum M_O=I\alpha\tag{39}$$

$$\begin{aligned}&-\left(F_L+F_R\right)l\cos\theta_p-\left(P_L+P_R\right)l\sin\theta_p\\&-\left(C_L+C_R\right)=I_p\ddot{\theta}_p\end{aligned}\tag{40}$$

The torque applied on the chassis from the motor as defined in Equation (40) and after linear transformation,

$$\left(C_L+C_R\right)=-\frac{2k_mk_e}{Rr}\dot{x}+\frac{2k_m}{R}V_s\tag{41}$$

Substituting this into Equation (40) gives,

$$\begin{aligned}&-\left(F_L+F_R\right)l\cos\theta_p-\left(P_L+P_R\right)l\sin\theta_p\\&-\left(-\frac{2k_mk_e}{Rr}\dot{x}+\frac{2k_m}{R}V\right)=I_p\ddot{\theta}_p\end{aligned}\tag{42}$$

Thus,

$$\begin{aligned}&-\left(F_L+F_R\right)l\cos\theta_p-\left(P_L+P_R\right)l\sin\theta_p\\&=I_p\ddot{\theta}_p-\frac{2k_mk_e}{Rr}\dot{x}+\frac{2k_m}{R}V_s\end{aligned}\tag{43}$$

By multiplying Equation (38) by –l,

$$\begin{aligned}&-\left[\left(F_L+F_R\right)l\cos\theta_p+\left(P_L+P_R\right)l\sin\theta_p\right]\\&+M_pl\,\mathrm{g}\sin\theta_p+M_pl^2\ddot{\theta}_p=-M_pl\ddot{x}\cos\theta_p\end{aligned}\tag{44}$$

Substitute Equation (43) in Equation (44),

$$\begin{aligned}&I_p\ddot{\theta}_p-\frac{2k_mk_e}{Rr}\dot{x}+\frac{2k_m}{R}V_s+M_pl\,\mathrm{g}\sin\theta_p\\&+M_pl^2\ddot{\theta}_p=-M_pl\ddot{x}\cos\theta_p\end{aligned}\tag{45}$$

To eliminate $\left(F_L+F_R\right)$ from the motor dynamics, Equation (36) is substituted into Equation (16),

$$\begin{aligned}&2\left[M_w+\frac{I_w}{r^2}\right]\ddot{x}=-\frac{2k_mk_e}{Rr^2}\dot{x}+\frac{2k_m}{Rr}V_s\\&-\left(M_pl\ddot{\theta}_p\cos\theta_p+M_pl\dot{\theta}_p^2\sin\theta_p+M_p\ddot{x}_R\right)\end{aligned}\tag{46}$$

$$\begin{aligned}&2\left[M_w+\frac{I_w}{r^2}\right]\ddot{x}=-\frac{2k_mk_e}{Rr^2}\dot{x}+\frac{2k_m}{Rr}V_s\\&-M_pl\ddot{\theta}_p\cos\theta_p+M_pl\dot{\theta}_p^2\sin\theta_p-M_p\ddot{x}_R\end{aligned}\tag{47}$$

Rearranging Equation (45) and Equation (46) gives the nonlinear equations of motion of the system.

$$\begin{aligned}&\left[I_p+M_pl^2\right]\ddot{\theta}_p-\frac{2k_mk_e}{Rr}\dot{x}+\frac{2k_m}{R}V_s\\&+M_pl\,\mathrm{g}\sin\theta_p=-M_pl\ddot{x}\cos\theta_p\end{aligned}\tag{48}$$

$$\begin{aligned}&\left[2M_w+\frac{2I_w}{r^2}+M_p\right]\ddot{x}+\frac{2k_mk_e}{Rr^2}\dot{x}\\&+M_pl\ddot{\theta}_p\cos\theta_p-M_pl\dot{\theta}_p^2\sin\theta_p=\frac{2k_m}{Rr}V_s\end{aligned}\tag{49}$$

The above two equations can be linearised by assuming $\theta_p=\pi-\phi$, where ϕ represents a small angle from the vertically upward direction. This simplification was used to enable a linear model to be obtained so linear state space controllers could be implemented.

Therefore,

$$\cos\theta_p=\cos\left(\pi-\phi\right)\approx-1\tag{50}$$

$$\sin\theta_p=\sin\left(\pi-\phi\right)\approx-\phi\tag{51}$$

$$\dot{\theta}_p=\dot{\phi}^2\approx0\text{ and }\ddot{\theta}_p=\ddot{\phi}\tag{52}$$

The linearised equation of motion is

$$\begin{aligned}&\left[I_p+M_pl^2\right]\ddot{\phi}-\frac{2k_mk_e}{Rr}\dot{x}+\frac{2k_m}{R}V_s\\&-M_pl\mathrm{g}\phi=M_pl\ddot{x}\end{aligned}\tag{53}$$

$$\begin{aligned}&\left[2M_w+\frac{2I_w}{Rr}+M_p\right]\ddot{x}+\frac{2k_mk_e}{Rr^2}\dot{x}\\&-M_pl\ddot{\phi}=\frac{2k_m}{Rr}V_s\end{aligned}\tag{54}$$

When Equation (53) and Equation (54) are rearranged, the state space equation of the system is obtained.

$$\begin{aligned}\ddot{\phi}=&\frac{M_pl}{\left(I_p+M_pl^2\right)}\ddot{x}+\frac{2k_mk_e}{Rr\left(I_p+M_pl^2\right)}\dot{x}\\&-\frac{2k_m}{R\left(I_p+M_pl^2\right)}V_s+\frac{M_pgl}{\left(I_p+M_pl^2\right)}\phi\end{aligned}\tag{55}$$

$$\begin{aligned}\ddot{x}=&\frac{2k_m}{Rr\left(2M_w+\frac{2I_w}{r^2}+M_p\right)}V_s\\&-\frac{2k_mk_e}{Rr^2\left(2M_w+\frac{2I_w}{r^2}+M_p\right)}\dot{x}\\&+\frac{M_pl}{\left(2M_w+\frac{2I_w}{r^2}+M_p\right)}\ddot{\phi}\end{aligned}\tag{56}$$

By substituting Equation (55) into Equation (49),

substituting Equation (43) into Equation (31), and after a series of algebraic manipulation, the state space equation for the system is obtained.

$$\begin{bmatrix} \dot{x} \\ \ddot{x} \\ \dot{\phi} \\ \ddot{\phi} \end{bmatrix} = \begin{bmatrix} 0 & 1 & 0 & 0 \\ 0 & \dfrac{2k_m k_e \left(M_p lr - I_p - M_p l^2\right)}{Rr^2\alpha} & \dfrac{M_p^2 gl^2}{\alpha} & 0 \\ 0 & 0 & 0 & 1 \\ 0 & \dfrac{2k_m k_e \left(r\beta - M_p l\right)}{Rr^2\alpha} & \dfrac{M_p gl\beta}{\alpha} & 0 \end{bmatrix} \begin{bmatrix} x \\ \dot{x} \\ \phi \\ \dot{\phi} \end{bmatrix} + \begin{bmatrix} 0 \\ \dfrac{2k_m \left(I_p + M_p l^2 - M_p lr\right)}{Rr\alpha} \\ 0 \\ \dfrac{2k_m \left(M_p l - r\beta\right)}{Rr\alpha} \end{bmatrix} V_s \tag{57}$$

$$y = \begin{bmatrix} 1 & 0 & 0 & 0 \\ 0 & 0 & 1 & 0 \end{bmatrix} \begin{bmatrix} x \\ \dot{x} \\ \phi \\ \dot{\phi} \end{bmatrix} + 0 \times V_s \tag{58}$$

Where,

$$\alpha = \left[I_p\beta + 2M_p l^2 \left(M_w + \frac{I_w}{r^2} \right) \right] \tag{59}$$

$$\beta = \left[2M_w + \frac{2I_w}{r^2} + M_p \right] \tag{60}$$

The detail descriptions for all mathematical expression are offered in the background theory of mobile robot system in several books.

In the abovementioned model, it is assumed that the wheels of the vehicle will always stay in contact with the ground and that there is no slip at the wheels. Therefore, cornering forces are also considered negligible.

3. Experimental Results and Discussions

The experimental results based on separated hardware implementation and overall system implementation were presented in this section. And also the outcomes of research are mentioned based on the discussions on several analyses.

3.1 Overall Operation of the System

The self-balancing two-wheeled robot is based on an inverted pendulum theory. Without any control system, it cannot maintain its upright position. To hold the robot in an excellent place, the controller should know at which angle the robot is tilting. This process can be done by the IMU sensor, which consists of a three-axis accelerometer and a three-axis gyroscope. The accelerometer is responsible for measuring the tilt angle, and the gyroscope shows the robot's angle position. However, each sensor data is not entirely accurate due to the presence of noise and drift in each sensor. To overcome this problem, a complementary filter is required to implement for fusing the sensor data. In this robot hardware, a control algorithm is written in an intelligent electronic device known as an Arduino UNO. UNO is used to collect the robot's orientation in a single axis from the IMU sensor and provide an appropriate control signal to control both left and suitable motor by tuning a Proportional, Integral and Derivative (PID) gain value. The output from this PID controller is a pulse width modulation (PWM) signal. Consequently, it can control the speed of the motor through a dual full-bridge motor driver (L298N). Thus to balance the two-wheeled self-balancing robot, tuning the PID gain values and filtering the sensor data play an essential role in this unstable system.

3.2 Closed-loop PID Controller Testing Based on Mathematical Model

PID controller is simulated in MATLAB/SIMULINK using the accurate parameter in the robot's mathematical model. The mathematical model equation was driven in Equation (56), and the robot's precise parameters have been calculated in section III.

Figure 4 demonstrates the Closed Loop Impulse Response of the System with PID. This simulation is constructed according to the state-space model. An impulse response is used to test the PID closed-loop control system. The first proportional gain (K_p=15) controls the position of the robot and the second PID controller controls the robot's angle. The input source is an impulse signal, and it is similar to the robot, which is suddenly pushed in the objective case. This impulse force will cause the robot to change its stable position and angle for a short period. The result can be seen in Figure 5.

Figure 5(a) means that the robot's position has changed from 0 meters to around 0.8 meters first due to the applied impulse force. This will create the robot to lean nearly 18 degrees. Consequently, the robot's angle must be controlled with proper PID gain values to maintain its

stability. Unless the robot's angle is held, it will fall. With the help of PID controllers in both position and angle, the robot will return to its initial position after 2 seconds, and at the same time, the robot's tilting angle will return to zero degrees. Among these two Figures 5(a) and 5(b), the right-hand side graph can give a better result when the robot's displacement and tilt angle measurements are compared.

In the second experiment, a unit step signal is used as an input to the system, and then the robot's position and angle are checked after passing through the PID controller in both cases. The main unsimilar point between Figure 4 and Figure 6 is the input signal. Figure 4 uses an impulse signal, while Figure 6 uses a unit step signal. The simulation result can be demonstrated in Figure 7. This time let's assume that the user wants to move the robot to one meter and stay in that position, like giving a unit step function to the robot's position in the simulation. In order to observe this, the robot should lean for at most around 15 degrees. With the help of these PID gain values, the robot could manage to reach that set point position within 3 seconds. After getting to the desired position, the robot's tilting angle will be returned to zero. In other words, the robot will return to its balanced position. Among these, two graphs the right-hand side graph can give a better result.

Last but not least, the PID controller is used to control only the robot's angle instead of the robot's position. MATLAB simulation diagram is shown in Figure 8.

This phenomenon is quite similar to setting the robot to lean forward to a certain degree constantly. The simulation result can be seen in Figure 9. In this simulation, the robot is set to lean forward for one degree constantly. Thus in Figure 9, at first, the robot is oscillating and trying to maintain in one degree; as a result, the robot will move continuously. Therefore, between these two figures: Figure 9(a) and Figure 9(b), Figure 9(b) can be assumed to be the best one by comparing the robot's angle graph.

One of the interesting facts in this simulation test is that all the PID gain values that are used in those three different simulations are the same value. This means that appropriate PID gain values for both unit step and unit impulse function in controlling both position and angle have already been tuned after realising the characteristic of the PID controller and trying a try and error method for tuning the gain values. Moreover, PID gain values used in every simulation (a) can balance the robot in software simulation and hardware testing.

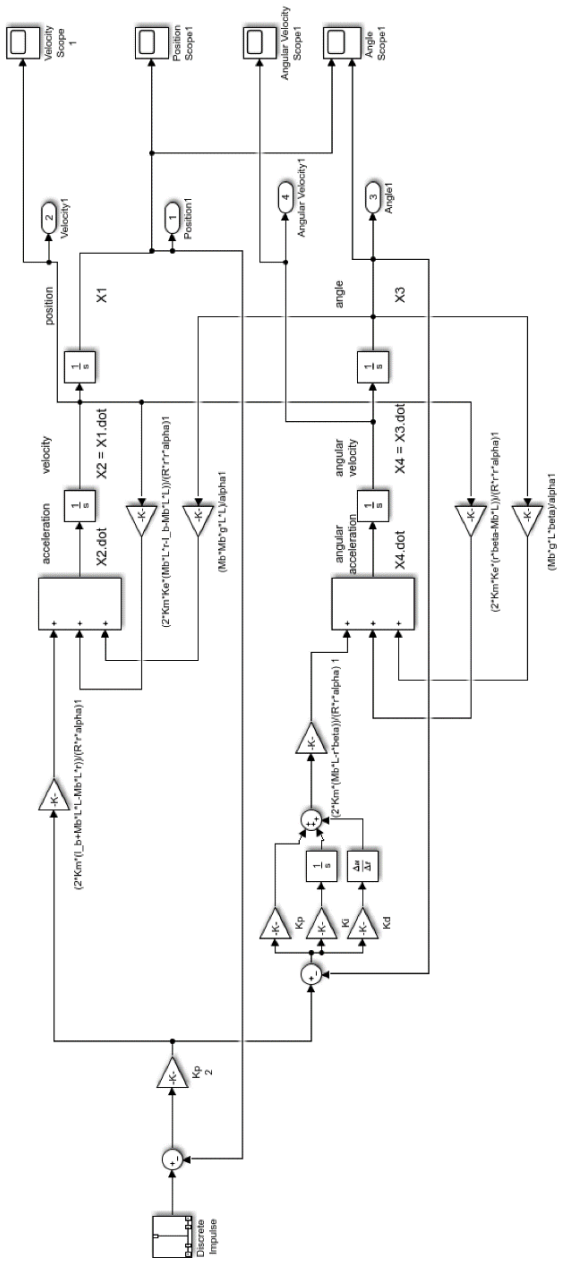

Figure 4. Closed Loop Impulse Response of the System with PID

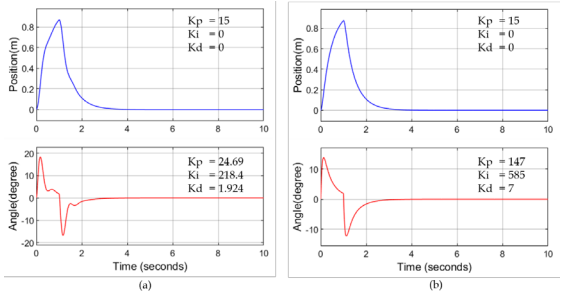

Figure 5. Test and Result of Closed Loop Impulse Response with PID Controller in Both Position and Angle

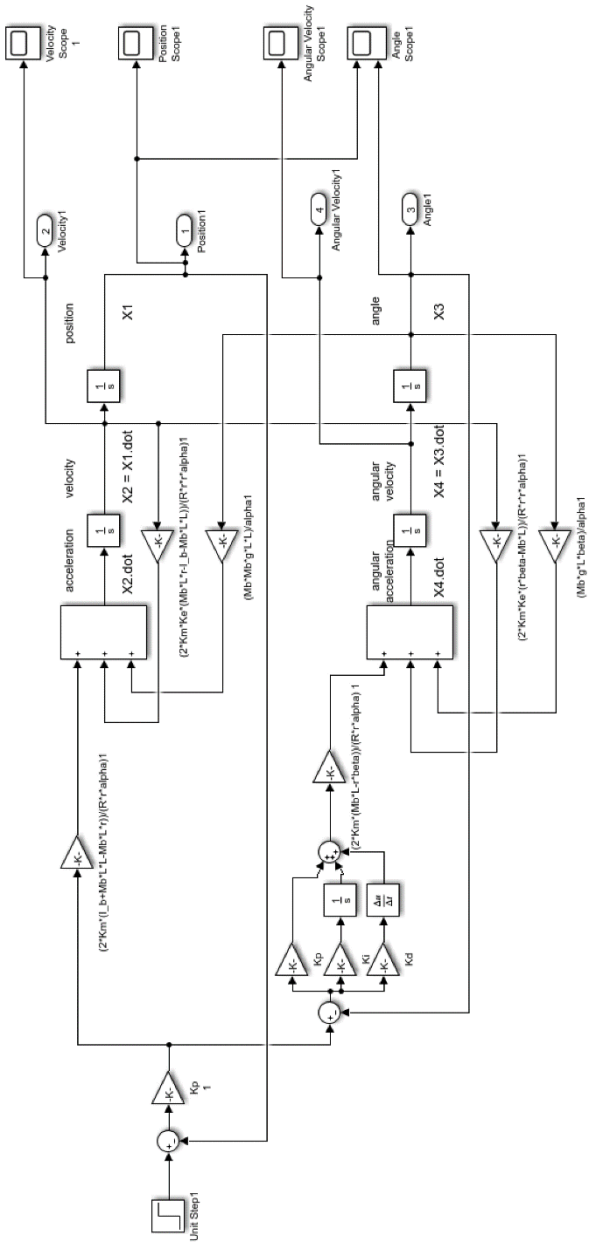

Figure 6. Closed Loop Unit Step Response of the System with PID Controller in Both Position and Angle

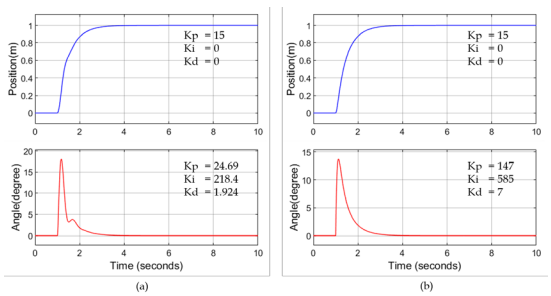

Figure 7. Test and Result of Closed Loop Unit Step Response with PID controller in Both Position and Angle

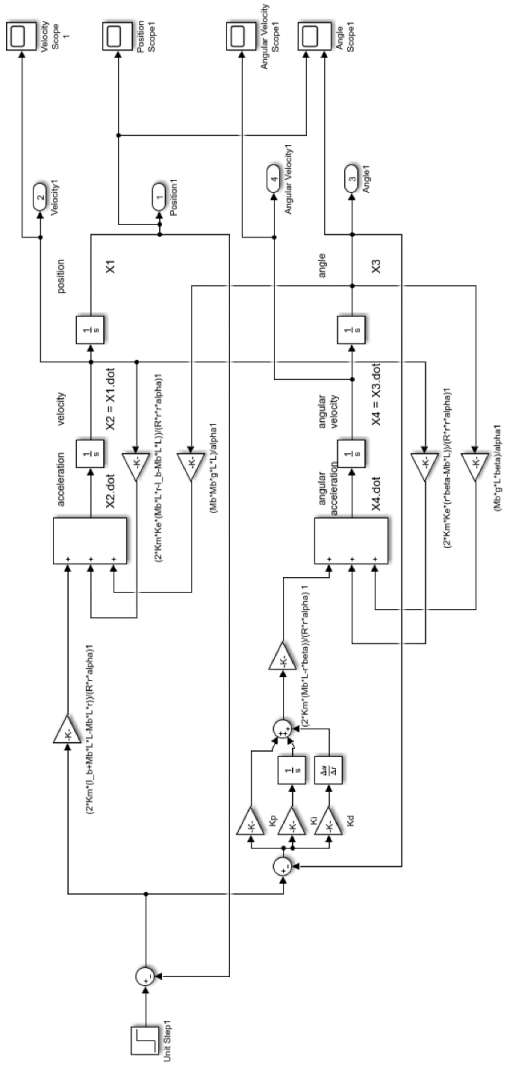

Figure 8. Closed Loop Unit Step Response of the System with PID Controller in Angle

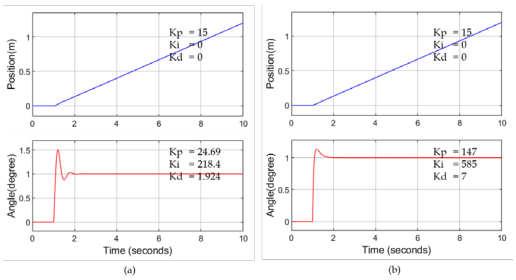

Figure 9. Test and Result of Closed Loop Unit Step Response with PID controller in Both Position and Angle

3.3 Closed Loop LQR Controller Testing Based on Mathematical Model

After substituting the robot's parameter into the state-space model derived in section III, Equation (60) is obtained.

$$\begin{bmatrix} \dot{x} \\ \ddot{x} \\ \dot{\phi} \\ \ddot{\phi} \end{bmatrix} = \begin{bmatrix} 0 & 1 & 0 & 0 \\ 0 & -113 & 10.81 & 0 \\ 0 & 0 & 0 & 1 \\ 0 & -630.4 & 178.2 & 0 \end{bmatrix} \begin{bmatrix} x \\ \dot{x} \\ \phi \\ \dot{\phi} \end{bmatrix} + \begin{bmatrix} 0 \\ 4.296 \\ 0 \\ 23.96 \end{bmatrix} V_s \quad (61)$$

For a linear control system to be implemented, the system has to be controllable. This requires that the rank of the $n \times n$ controllability matrix $C = \left[BAB...A^{n-1}B \right]$ is n or modulus of C is not equal to zero.

The algebraic Ricatti equation is solved using MATLAB, and the control gain K is evaluated for different values of Q and R weighting matrices. The response of the system is simulated as well.

The Q matrix assumes the form of

$$Q = \begin{bmatrix} a & 0 & 0 & 0 \\ 0 & b & 0 & 0 \\ 0 & 0 & c & 0 \\ 0 & 0 & 0 & d \end{bmatrix} \quad (62)$$

where the values of a, b, c and d are the weightings for the states $x, \dot{x}, \phi, \dot{\phi}$ while the weighing matrix R is a scalar value as there is only one control input to the system. The values in Q and R matrices are adjusted to penalise the system state space and input. The main aim of this control system is to make the states of the system converge to zero at the shortest time possible. Thus the control engineer should adjust the Q and R matrices to obtain the desired response. The simulation result for this self-balancing robot is illustrated in Figure 10.

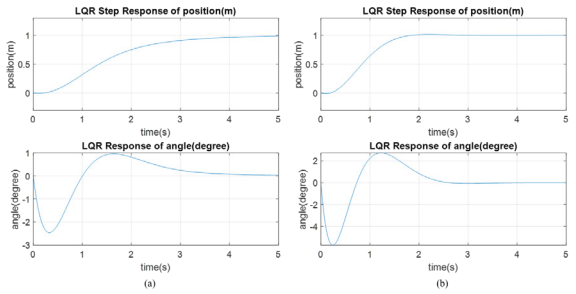

Figure 10. Test and Result of Closed Loop LQR controller

Figure 10(a) uses a=10, b=10, c=60, d=100 for Q matrix and R=0.001. Using these values, the robot will reach the desired position 1m after 4 seconds by oscillating the robot between –2 degrees and 1 degree. Figure 10(b) uses a=100, b=10, c=600, d=100 for Q matrix and R=0.001. At these values, the robot will reach the desired position 1 m after 2 seconds by oscillating the robot between –5 degrees and 2.3 degrees. Among these two LQR simulations, Figure 10(b) can provide better performance than that of (a). Moreover, by comparing this LQR simulation result (b) with the PID control simulation result in Figure 7(b), the LQR controller can perform better because the robot will reach the desired distance of 1 meter within 2 seconds the tilting angle of a maximum 5 degrees. But with the PID control, the robot needs to tilt about 15 degrees to reach the desired position within 2 seconds.

3.4 Flowchart of the Robot Control System

The flowchart used to carry this project can be seen in Figure 11. Once the necessary components are set, the operation of the flowchart will be explained in this section.

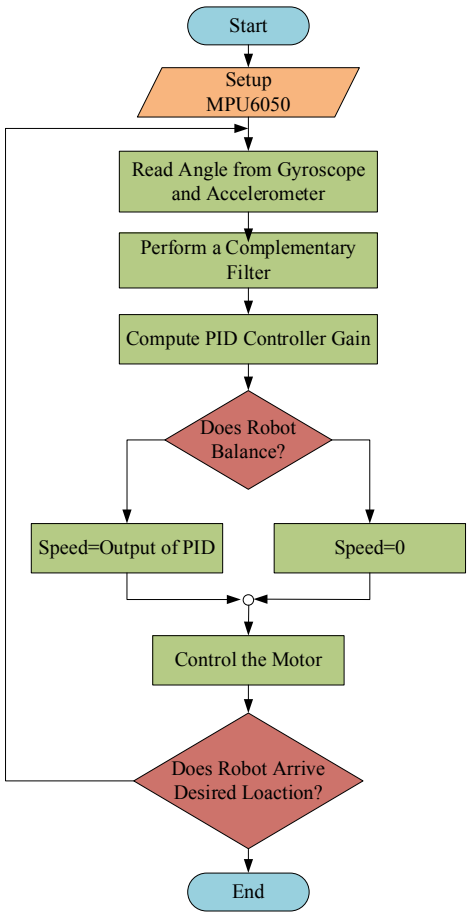

Figure 11. Flowchart of the Robot Control System

First of all, the MPU6050 sensor is initialised in the setup function. After that, the accelerometer and gyroscope raw data are acquired from the sensor and then passed through the complementary filter to remove drift and noise from MPU6050. Then, it is sent to the PID controller. By tuning the PID gain values, the motor speed can be controlled with a PWM signal. If the sensor senses that the robot is in a balanced condition, the PID controller

will command the motor not to move for ten milliseconds which becomes the system's loop time. When the sensor senses that the robot is tilting forward for five degrees, the PID controller will command the motor to accelerate the motor forward until the robot becomes stable. In this way, the robot can balance itself successfully. Finally, when battery power is not enough, the robot will stop running [16]. The specific coding is not mentioned in this paper.

3.5 Hardware Testing

To implement the flowchart program in the hardware properly. Getting angle from the MPU6050 sensor is the first priority for hardware testing.

The Arduino Uno communicates with the MPU6050 through the I2C protocol. Thus serial clock pin (SCL) is connected to the Arduino (A5) pin as well as the serial data pin (SDA) is connected to the Arduino (A4) pin. The sensor's interrupt pin (INT) is then connected to the Arduino pin2. Arduino supplies 3.3V to the sensor by connecting the Vcc pin from the sensor and the 3V3 pin from the Arduino. The two ground pins are made sure to communicate with each other.

After interfacing the sensor and Arduino Uno, the program should be uploaded to test the sensor. Then the raw data are saved in the excel file and plotted in MATLAB. After that, check the nature of the accelerometer and gyroscope sensor and perform complementary in MATLAB code.

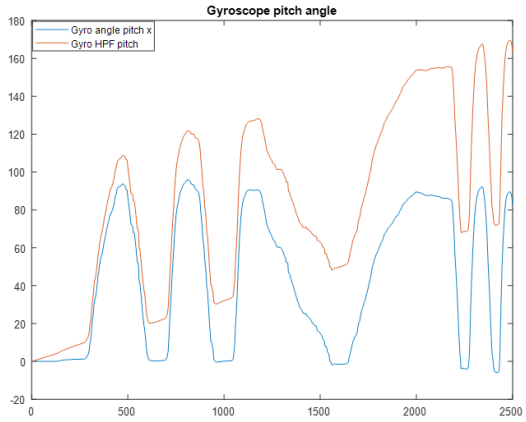

Figure 12. Gyroscope Pitch Angle

The sensor is rotated only in one axis (pitch angle) from 0 to 90 degrees and then rotates again from 0 to 90 degrees for another four times. In Figure 12, the blue line represents the gyroscope pitch angle, and the red line represents the gyroscope high pass filter pitch angle. It was evident that the gyroscope has a bias. Thus without passing a high pass filter, the sensor data are drift gradually. However, in the filtered data, a small drift still presents in between 2000 and 2500 samples.

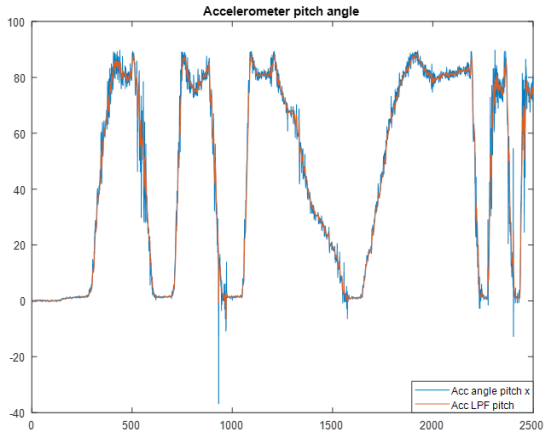

Figure 13. Accelerometer Pitch Angle

Figure 13 represents the nature of the accelerometer sensor. The blue line represents the accelerometer pitch angle, and the red line represents the accelerometer low pass filter pitch angle. Even there is no bias in the accelerometer, and it is pretty sensitive to noise. As a result, a low pass filter is needed to filter out this noise. Moreover, even the sensor is rotated from 0 to 90 degrees for six times, the accelerometer sensor data and low pass filtered data cannot represent absolute 90 degrees when only the accelerometer sensor is used to calculate the angle.

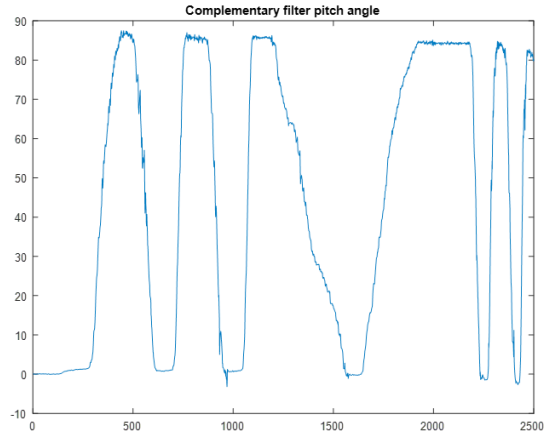

Figure 14. Complementary Filter Pitch Angle

In order to solve the problem occurring in both accelerometer and gyroscope sensors, a complementary filter is used to get a better result. For example, Figure 14 combines the two sensors' data, and this filter is designed to trust the gyroscope sensor data more than that of the accelerometer.

3.6 Implementing PID Controller to the Robot Control System

After testing each component before implementing the whole system, the PID control algorithm is written in the Arduino. This PID controller plays an essential role in the self-balancing robot system. The reason is that without a controller or a poor control design, the robot cannot balance itself and is stable in one position. Thus, in this case, tuning the PID controller plays an important role. Therefore, the author did a lot of experiences to get the perfect controller gain values. Among them, four different PID gain values are selected.

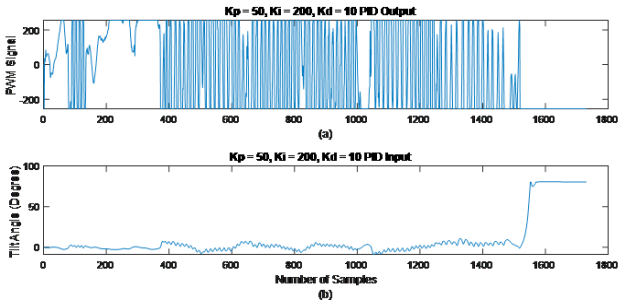

Figure 15. The First PID Tuning in Robot

Figure 15 shows all data conditions of the running robot with PID gain values of K_p = 50, K_i = 200 and K_d = 10. Figure 14(a) represents the PID output (PWM signal) to control the motor speed. Figure 14(b) illustrates the robot's actual tilting angle. In this Figure 14, the robot cannot keep in a balance position because it falls down after operating for a short period. This phenomenon can be seen when the robot's tilting angle reaches 90 degrees.

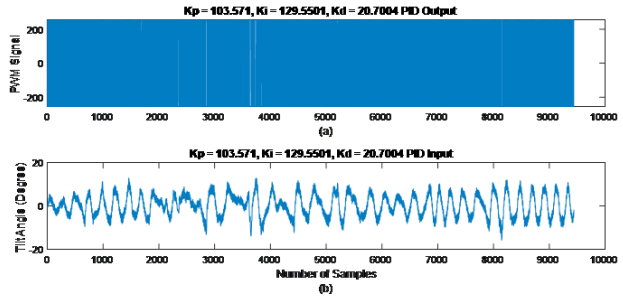

Figure 16. The Second PID Tuning in Robot

Since PID gain values in Figure 14 cannot maintain the robot in an upright position, other PID gain values are tuned. Figure 16 shows all data conditions of the running robot with PID gain values of K_p = 103.571, K_i = 129.5501, and K_d = 20.7004. Figure 15(a) represents the PID output (PWM signal) to control the motor speed. Figure 16(b) illustrates the robot's actual tilting angle. These gain values make the robot oscillate a lot; as a result, the PID controller needs to work at a maximum and a minimum limit of +255 and –255 PWM signals during the running condition. However, it cannot maintain the robot in a stable condition.

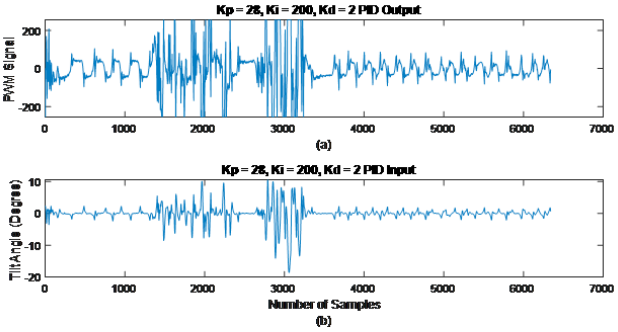

Figure 17. The Third PID Tuning in Robot

Thirdly, PID gain value is changed into K_p = 28, K_i = 200, and K_d = 2. Then the robot's condition is checked. Unlike Figure 16, the PID controller does not need to work at a maximum or minimum limit apart from a disturbance. These gain values can keep the robot in a stable condition since, in Figure 17(b), the robot does not tilt a lot without a disturbance.

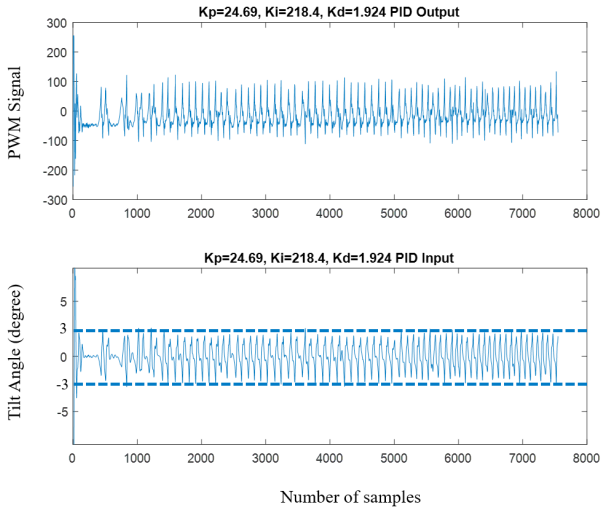

Figure 18. The Balancing Condition of the Robot in Upright Position

This final PID gain value of K_p = 24.69, K_i = 218.4; and K_d = 1.924 can improve the robot's stability. The robot oscillates between –3 degrees and 3 degrees during the experiment. This means that the PID controller controls the motor driver not to let the robot tilt beyond 3 degrees. Thus it can be concluded that this gain value can provide a more stable condition for the self-balancing robot. The result can be seen in Figure 18.

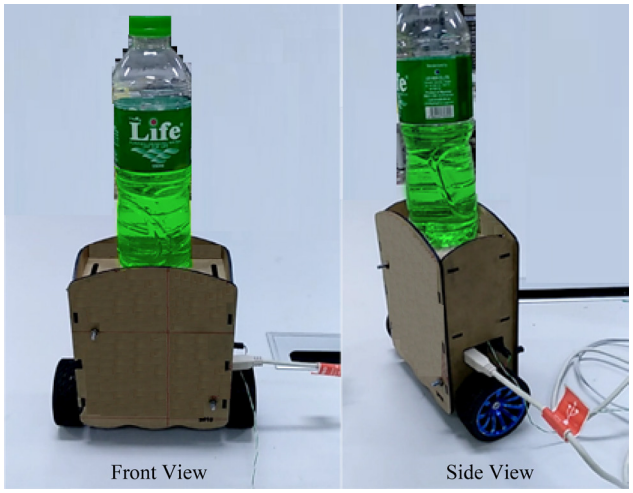

Figure 19. The Balancing Condition of the Robot in the Presence of Extra Weight

Moreover, to know whether this PID gain value of K_p = 24.69, K_i = 218.4; and K_d = 1.924 can maintain the robot's stable condition or not when extra weight is applied to it, a half-filled 0.6 litre of water bottle is placed at the top of the robot's chassis and run the robot. Therefore, this PID controller can also maintain the robot in a stable condition. The front and side view of the robot's running condition can be seen in Figure 19. In order to get this PID to gain value, many experiments are tested during the research program. The simulation tools in this mathematical modelling are based on the MATLAB and Arduino programming. The accuracy could be checked by using the ratio of difference between real and defined position to the defined position in this study.

3.7 Challenging Issues

During this research, a minor challenging issue appeared, such as resizing the depth of the robot chassis because the laser cutter cuts the acrylic sheets into 2 mm instead of cutting into 3mm sheets. However, one major issue was found with the DC motors employed: the first motor, GM25-370-24140 DC motor, does not have enough RPM to rotate when the robot turns to tilt into a large angle. For this reason, it is so complicated to tune the PID control. Fortunately, this problem is solved by replacing it with a 500RPM DC motor.

3.8 Discussions

This research work successfully achieves the goals of balancing unstable two-wheeled robots. Balancing an unstable system is a challenging problem in the research field, and the various controllers can be used in stabilising the system. In this research work, PID and LQR controller is used to control the robot's position and angle. But in hardware testing, only PID controller is used. First, the 3D design of the self-balancing robot was drawn in the Solid Works software to find the best location for each electronic component. By doing so, the author does not have any problem with hardware assembling in practice. Next, the complementary filter has been successfully implemented to filter a gyroscope drift and accelerometer noise, allowing for an accurate estimation of the robot's tilting angle. Arduino must communicate the IMU sensor via I2C communication and control the motor's speed via PWM signal. After passing the filtered sensor data to the microcontroller, the microcontroller compares the actual tilting angle with the setpoint value to check the error. This error is compensated by using a PID controller in hardware. Both PID and LQR control algorithms have successfully compared the software simulation result in MATLAB using the robot's state-space model. LQR can provide better performance than the PID controller. Due to the time limit, only the PID controller is successfully implemented to address the problem of balancing an unstable system in hardware testing. But this PID tuned values of K_p = 24.69, K_i = 218.4, and K_d = 1.924 used in hardware can maintain the robot upright on flat surfaces. Moreover, it can control the robot in a balanced condition with extra weight, as shown in Figure 18. Last but not least, this gain value is also satisfied in software simulation. Therefore, many experiments and simulations were done to achieve a better result. This work is novel for emphasizing on the numerical approaches for experimental approaches with discrete components and utilizing the fundamental concepts of the dynamic control system design. The performance comparison on the mobile robot system was depending on the controller design and robustness of the system. That is the innovative work in this study.

3.9 Limitations

The limitations of the developed mobile robot system are latency of the control signal input to the process by controller output and the translational vector between the simulation approaches to experimental approaches. The problem could be solved to acquire the better performance for experimental studies with the speed of controller design and optimal gain tuning is the contribution in this work.

4. Statistics Table for Results Comparison

The experimental results of self-balancing mobile robot system in this study and recent works are given in the following Table 1. The performance comparisons are found in this table with various kinds of conditions.

Table 1. Performance Comparison Table

Works	Controller Design	Accuracy	Performance Level	Robustness
[17]	PD	93%	High	Satisfy
[18]	LQR	94%	High	Satisfy
[19]	PWM	90%	Medium	Satisfy
This Work	PID and LQR	98%	Very High	Satisfy

The control algorithm is based on the real time control system for specific analysis. The application of the mobile robot system is for healthcare service in real time conditions.

5. Conclusions

This research successfully achieved its aims to balance a self-balancing robot based on the inverted pendulum model. Two control strategies have been implemented to address the problem of balance control for the system. The gain matrices obtained from PID simulation are implemented in this self-balancing robot for real-time controller experimentation. During the testing, the robot can maintain its vertical position by slightly adjusting its wheels. Besides PID control, the LQR controller is also successfully tested in MATLAB simulation. The PID controller can easily be tuned by observing the optimal condition. The LQR controller can also better results when the Q matrix and R matrix are adequately set. Many simulations are run to get the best result for this self-balancing robot. In the hardware testing, the PID controller is designed to control a single axis robot tilting angle, y-axis. Rotating in both x and z axes is neglected in implementing the PID control algorithm because this research work focuses only on stabilizing the robot. Also, controlling the position is not considered in hardware testing. However, in MATLAB simulation, both PID and LQR are considered in controlling both robot's position and angle. Thus, considering the yaw axis and x y movement is recommended for trajectory tracking in the robot's hardware. So that later formation control can be performed. Stabilizing the robot on a sloped area and a rough surface area is recommended as a further extension. PID controller cannot maintain stable conditions for slopes and rough surfaces. Thus apart from PID controller, Linear Quadratic Regulator (LQR), pole-placement, fuzzy control, adaptive control, sliding mode control (SMC), etc., are recommended to implement in this robot to decide which controller can perform the best in the future development of the self-balancing robot. Moreover, a manual remote control system like commanding the robot to move forward, backwards and rotate clockwise or counter-clockwise direction via Bluetooth wireless connection can also be considered in this self-balancing robot. The numerical expressions were matched to the experimental studies in this study based on the accuracy percentage of 98%. The performance level is also very high by comparing with the other recent works.

Conflict of Interest

There is no conflict of interest.

Acknowledgment

The authors acknowledge researchers and colleagues from the Faculty of Electrical and Computer Engineering of Yangon Technological University. This work is fully supported by Government Research Funds for 2021-2022 Academic Year. This work is completely measured and analyzed at the Electrical and Electronics Properties Evaluation Laboratory Room (EB-402) of the Myanmar Japan Technological Development Centre 1 (MJTDC 1) of Yangon Technological University (YTU). This work is collaborative research work with Acharya Institute of Technology in India and Chulalongkorn University in Thailand.

References

[1] Peng, K., Ruan, X., Zuo, G., 2012. Dynamic model and balancing control for two-wheeled self-balancing mobile robot on the slopes. Proceedings of the 10th World Congress on Intelligent Control and Automation. pp. 3681-3685. (Accessed 9 September 2021). DOI: https://doi.org/10.1109/WCICA.2012.6359086

[2] Bin, H., Zhen, L.W., Feng, L.H., 2010. The Kinematics Model of a Two-Wheeled Self-Balancing Autonomous Mobile Robot and Its Simulation. 2010 Second International Conference on Computer Engineering and Applications. pp. 64-68. (Accessed 18 September 2021). DOI: https://doi.org/10.1109/ICCEA.2010.169

[3] Gong, D., Li, X., 2013. Dynamics modeling and controller design for a self-balancing unicycle robot. Proceedings of the 32nd Chinese Control Conference. pp. 3205-3209. (Accessed 27 September 2021).

[4] Nikita, T., Prajwal, K.T., 2021. PID Controller Based Two Wheeled Self Balancing Robot. 2021 5th International Conference on Trends in Electronics and Informatics (ICOEI). pp. 1-4. (Accessed 8 October 2021). DOI: https://doi.org/10.1109/ICOEI51242.2021.9453091

[5] Philip, E., Golluri, S., 2020. Implementation of an Autonomous Self-Balancing Robot Using Cascaded

PID Strategy. 2020 6th International Conference on Control, Automation and Robotics (ICCAR). pp. 74-79. (Accessed 9 September 2021).
DOI: https://doi.org/10.1109/ICCAR49639.2020.9108049

[6] Jianwei and Xiaogang, 2008. The LQR control and design of dual-wheel upright self-balance Robot," 2008 7th World Congress on Intelligent Control and Automation. pp. 4864-4869. (Accessed 9 September 2021).
DOI: https://doi.org/10.1109/WCICA.2008.4593712

[7] Yu, N., Li, Y., Ruan, X., et al., 2013. Research on attitude estimation of small self-balancing two-wheeled robot. Proceedings of the 32nd Chinese Control Conference. pp. 5872-5876. (Accessed 9 September 2021).

[8] Putov, A.V., Ilatovskaya, E.V., Kopichev, M.M., 2021. Self-balancing Robot Autonomous Control System. 2021 10th Mediterranean Conference on Embedded Computing (MECO). pp. 1-4. (Accessed 9 September 2021).
DOI: https://doi.org/10.1109/MECO52532.2021.9459720

[9] Sarathy, S., Mariyam Hibah, M.M., Anusooya, S., et al., 2018. Implementation of Efficient Self Balancing Robot. 2018 International Conference on Recent Trends in Electrical, Control and Communication (RTECC). pp. 65-70. (Accessed 9 September 2021).
DOI: https://doi.org/10.1109/RTECC.2018.8625624

[10] Sun, W.X., Chen, W., 2017. Simulation and debugging of LQR control for two-wheeled self-balanced robot. 2017 Chinese Automation Congress (CAC). pp. 2391-2395. (Accessed 9 September 2021).
DOI: https://doi.org/10.1109/CAC.2017.8243176

[11] Ruan, X.G., Liu, J., Di, H.J., et al., 2008. Design and LQ Control of a two-wheeled self-balancing robot. 2008 27th Chinese Control Conference. pp. 275-279. (Accessed 9 September 2021).
DOI: https://doi.org/10.1109/CHICC.2008.4605775

[12] Lv, Q., Wang, K.K., Wang, G.Sh., 2009. Research of LQR controller based on Two-wheeled self-balancing robot. 2009 Chinese Control and Decision Conference. pp. 2343-2348. (Accessed 9 September 2021).
DOI: https://doi.org/10.1109/CCDC.2009.5192771

[13] Kongratana, V., Gulphanich, S., Tipsuwanporn, V., et al., 2012. Servo state feedback control of the self balancing robot using MATLAB. 2012 12th International Conference on Control, Automation and Systems. pp. 414-417. (Accessed 9 September 2021).

[14] Gong, Y., Wu, X., Ma, H., 2015. Research on Control Strategy of Two-Wheeled Self-Balancing Robot. 2015 International Conference on Computer Science and Mechanical Automation (CSMA). pp. 281-284. (Accessed 9 September 2021).
DOI: https://doi.org/10.1109/CSMA.2015.63

[15] Tun, H.M., Nwe, M.S., Naing, Z.M., 2008. Design analysis of phase lead compensation for typical laser guided missile control system using MATLAB bode plots. 2008 10th International Conference on Control, Automation, Robotics and Vision. pp. 2332-2336. (Accessed 9 September 2021).
DOI: https://doi.org/10.1109/ICARCV.2008.4795897

[16] Tun, H.M., Nwe, M.S., Naing, Z.M., et al., 2022. "Sliding Mode Control-Based Two Wheels Mobile Robot System", The 14th Regional Conference on Electrical and Electronics Engineering (RC-EEE 2021), Chulalongkorn University, Thailand. (Accessed 9 January 2022).

[17] Velagic, J., Kovac, I., Panjevic, A., et al., 2021. Design and Control of Two-Wheeled and Self-Balancing Mobile Robot. pp. 77-82.
DOI: https://doi.org/10.1109/ELMAR52657.2021.9550938

[18] Pajaziti, A., Gara, L., 2019. Navigation of Self-Balancing Mobile Robot Through Sensors. IFAC Papers Online. 52-25, 429-434.
DOI: https://doi.org/10.1016/j.ifacol.2019.12.576

[19] Chhotray, A., Pradhan, M.K., Pandey, K.K., et al., 2016. Kinematic Analysis of a Two-Wheeled Self-Balancing Mobile Robot. Proceedings of the International Conference on Signal, Networks, Computing, and Systems, Lecture Notes in Electrical Engineering. Springer India. 396.
DOI: https://doi.org/10.1007/978-81-322-3589-7_9

BILINGUAL PUBLISHING CO.
Pioneer of Global Academics Since 1984

Electrical Science & Engineering
https://ojs.bilpublishing.com/index.php/ese

ARTICLE

Water Manipulation through Curvature Energy on Humidity Microparticles

Francisco Bulnes* **Isaías Martínez** **Isaí M. Martínez**

IINAMEI, International Advanced Research in Mathematics and Engineering, C. A. Chalco, Mexico

ARTICLE INFO

Article history
Received: 16 March 2022
Revised: 10 April 2022
Accepted: 17 April 2022
Published Online: 25 April 2022

Keywords:
Curvature energy
Humidity
Mean energy curvature
Spectral curvature
Stereo-radially
Water particles

ABSTRACT

The electric field created in a curvature energy sensor on air microparticles is used to obtain a temperature-humidity map $\mathsf{G}: M \to SO(2) \cup F$, by stereo-radially of the sensor design to detect and measure the temperature and humidity of certain local region of the environment space. Likewise, considering the curvature energy as the deviation of any field interaction, even the obstruction to its proper flow, is designed and created a humidity-resistor sensor to the control and optimization of humidity in a space with different gradients of humidity, pressure and temperature in a radial detection and measuring. Then the sensing problem is a problem of free boundary conditions where is satisfied an energy functional of norm $\|\xi\|_2$, to curvature functions κ, that satisfy in the temperature and humidity function ξ, the change limit condition $\xi|_{\partial\Omega} \leq 2\pi\xi(r)$. This carries to that the temperature-humidity sensor must be designed on a length gauge to measure the changes of humidity and temperature in the space.

1. Introduction

Let $M \subset \mathsf{R}^3$, a space where we want to detect and measure the humidity and temperature considering the humidity micro-particles in the air of an environment bounded to the boundary conditions of an electromagnetic field of managing and geometrical design of the proper sensor to optimizing and measuring of sensed with several research and application goals:

i) Measurement and detection in a region, at least of certain kilometers of radius, of the humidity and temperature to realize a distribution map of these characteristics. This will come considering the humidity micro-particles in the air of the environment, directly.

ii) The managing of water microparticles to their storage and use.

iii) The obtaining of energy through curvature energy to diverse uses and applications. For example, to energy transducer through humidity microparticles.

The goal iii) will be realized in the second part of this

*Corresponding Author:
Francisco Bulnes,
IINAMEI, International Advanced Research in Mathematics and Engineering, C. A. Chalco, Mexico;
Email: francisco.bulnes@tesch.edu.mx

DOI: https://doi.org/10.30564/ese.v4i1.4529

research although will be given the bases to its development.

Likewise, is necessary consider the general thermic-pressure-humidity process described under the framework of differential equations [1]:

$$\frac{d\boldsymbol{\upsilon}}{dt} = -\alpha\nabla P - \nabla\varphi + \boldsymbol{F} - 2\boldsymbol{\Omega}\times\boldsymbol{\upsilon}, \tag{1}$$

$$\frac{\partial\rho}{\partial t} = -\nabla\bullet(\rho\boldsymbol{\upsilon}), \tag{2}$$

$$P\alpha = RT, \tag{3}$$

$$Q = C_P\frac{dT}{dt} - \alpha\frac{dP}{dt}, \tag{4}$$

$$\frac{\partial pq}{\partial t} = -\nabla\bullet(\rho\boldsymbol{\upsilon}q) + \rho(E - C), \tag{5}$$

where the humidity phenomena depends on the temperature and pressure of the system of interest.

Likewise from (1)-(5), $\boldsymbol{\upsilon} = (\upsilon_x, \upsilon_y, \upsilon_z)$, is the velocity field of the gas, $q = T(t)$, and $p = P(t)$, is the temperature and pressure functions depending of time, $\rho = \frac{1}{\alpha}$, (with $\alpha = \mathrm{V}/nR$)① is the gas density, Q, is a heat.

In this case, the gas will be the air.

We consider a mass constant of sensing, thus from (2) we have

$$\frac{\partial\rho}{\partial t} = 0, \qquad \rho\nabla\boldsymbol{\upsilon} = 0, \tag{6}$$

and the general law gas is reduced to the law $P/T = cte$, where volume of the air sensor sample is constant [2].

The humidity is a function of two gas state variables, the temperature and pressure, which are time functions. Likewise, the humidity is the 2-dimensional surface:

$$\xi = \xi(T(t), P(t)), \tag{7}$$

The function (7) will be used in the spectral study of the humidity through humidity sensor outputs whose frequency variation will be useful to conform a stereo radial mapping of the environment to a scale factor captured through humidity, temperature and pressure signals, which combining will obtain a energy spectra of humidity.

Under certain constant volume of air with high content of water steam,② we have the following criteria to behavior of the function ξ,

i) If $T \to \infty$, then $P \to 0$, and the humidity $\xi \to \infty$, thus the clime is humid.

ii) If $T \to 0$, then $P \to \infty$, and the humidity $\xi \to 0$, thus the clime is dry.

Likewise, we consider the sensor chip to obtain directly pressure and temperature through humidity gradient with:

$$X_\xi = -\mathrm{grad}\,\xi(T, P), \tag{8}$$

We obtain inside an isochoric semi-spherical region that:

$$\mathrm{div}\nabla\xi = \nabla^2\xi = 2\pi\rho = cte, \tag{9}$$

with the corresponding spherical coordinates system, because has been chosen a semi-sphere as region where will be located the humidity sensor in its center (see the Figure 1). Here must be satisfied the Poisson equation to constant distribution of air. Then the sensing will be using the curvature energy, and the radial detection of the airflow to measure their humidity and temperature. This optimizes the sensoring and detection of humidity and temperature.

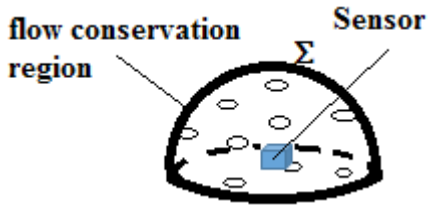

Figure 1. Flow conservation-detection region.

Likewise, from the energy equation (5) we have in energy-interchange due mass that :

$$E = C, \tag{10}$$

Then the energy flow satisfies that:

$$\frac{\partial pq}{\partial t} = -\rho\nabla(\tilde{\boldsymbol{\partial}}q), \tag{11}$$

which para a local coordinates system, (11) can be re-write as:

$$\begin{aligned}&\left[\frac{\partial P}{\partial x}\frac{dx}{dt} + \frac{\partial P}{\partial y}\frac{dy}{dt} + \frac{\partial P}{\partial z}\frac{dz}{dt}\right]\\ &+\left[\frac{\partial q}{\partial x}\frac{dx}{dt} + \frac{\partial q}{\partial y}\frac{dy}{dt} + \frac{\partial q}{\partial z}\frac{dz}{dt}\right] =\\ &-\rho\left(\frac{\partial\upsilon_x}{\partial x}q + \frac{\partial\upsilon_y}{\partial y}q + \frac{\partial\upsilon_z}{\partial z}q\right),\end{aligned} \tag{12}$$

which establish the energy interchange of the flow conservation-detection region of the sensor in the 3-dimensional space.

Likewise, we consider (7) and we take an isochoric process with constant pressure given by the atmospheric (barometric) pressure of the place. Then (7) takes the form:

$$\xi = P\xi(T(t), 1) = P\xi(T(t)), \tag{13}$$

Likewise its variation respect to time will be:

① Likewise, the general gas law is $PV = nRT$. If $\rho = cte$, then we have the classical general gas law form: $\frac{P\mathrm{V}}{T} = cte$. Here R, is the Boltzmann constant ($1.381\times10{-}23\ \mathrm{J\cdot K^{-1}}$), n, is the number of gas molecules.

② The volumen of humidity

$$P\frac{d\xi(T(t))}{dt} = P\frac{d\xi(T(t))}{dT}\frac{dT}{dt}, \tag{14}$$

However, we are interested in the humidity as state function, thus we consider the variation of humidity respect to temperature and pressure (but pressure is constant), proportional to it-self humidity with respect to pressure and volume constants:

$$P\frac{d\xi(T)}{dT} = k\xi(T), \tag{15}$$

with initial condition $\xi_{ext}(T_0) = \xi_{int}(T_0)$, where $T_0 \pm \Lambda$, depending of the increasing or decreasing of temperature and measure scale.

Likewise the general law that will govern the physical process of humidity is:

$$\xi(T) = \xi(T_0)e^{k(T-T_0)}, \tag{16}$$

Here the constant $\xi(T_0)$ ③ involves the barometric pressure, the volume of the scale region, the rate of relative humidity diffusion and other constants relative to the relative humidity④.

We want to detect the functions $\xi(T)$, as energy signals to the sensoring process, inside a region where is satisfied the Poisson equation (9) to air density or distribution ρ.

Due to the electronic component of our humidity sensor only can be installed with its receptor in one direction, we need consider a surface Σ, whose speed of direction change can be taken in the inner and consigned by electronic signals of energy accord to its geometrical invariant [3]. Then we require curvature energy [4-6].

However, what curvature energy? This will be from a normal curvature obtained. Why?

The flow conditions and behavior of the air without enclosure Σ, no reflects an ordered behavior of the air then cannot be sensed and detected by humidity sensor (see the Figure 2A), even in disclosure conditions the airflow cannot be bounded for electronics parameters range. Then we need an enclosure given by Σ (see the Figure 2B).

The perfect enclosure Σ, will be the geometrical enclosure, which can establish permanent conditions of the humidity field as has been established in (8) and whose boundary conditions no vary and have not different direction in inputs inside the enclosure (Figure 2B).

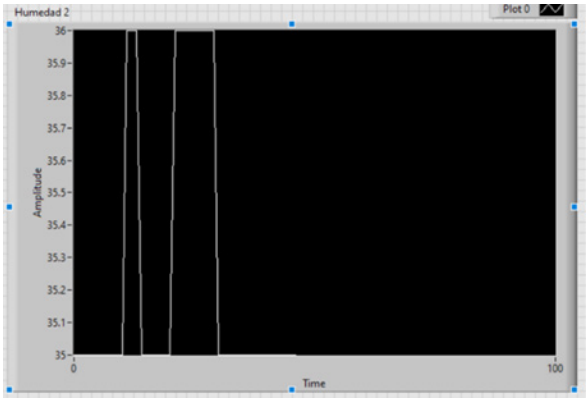

A. without spherical dome or enclosure with air flow

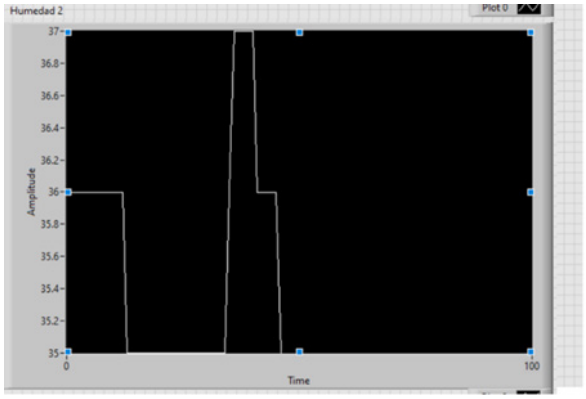

B. with spherical dome or enclosure with air flow

Figure 2. Temperature and humidity.

Likewise, the air inputs-outputs through of enclosure must be radials and obey the following boundary conditions:

$$\xi\big|_{\Sigma} \le 2\pi\xi(r), \tag{17}$$

which only has meaning in a spherical symmetry. Thus we choice a spherical dome where we consider the positive hemisphere (see the Figure 3).

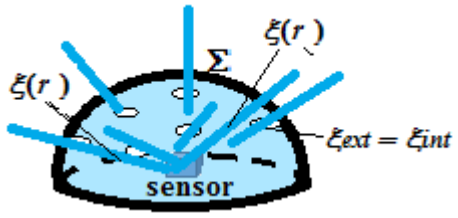

Figure 3. Air inputs-outputs through of enclosure must be radials.

Then an interesting conjecture derived directly of the chosen geometry to the sensor is:

Conjecture 1. 1. The radial humidity signal is 2π units its normal curvature.

③ $\xi(T_0) = \frac{V\phi}{nRT}K$, where K, is the characteristic function defined to the enclosure or sensing region which is a semi-sphere.

④The relative humidity of an air-water mixture is defined as the ratio of the partial pressure of water vapor in the mixture to the equilibrium vapor pressure of water over a flat surface of pure water [7] at a given temperature.

2. Some Simple Experiments of Field of the Humidity Sensor with Geometrical References

Considering the mentioned in the section 1, we have the following lemma to analyze from a geometrical point of view, the reception of signals by sensor, and geometrical disposition of this.

Lemma 2. 1. The detection and measurement of humidity will be through the normal curvature of the surface Σ, which is its Radon transform [8].

Proof. We consider as characteristic function of curvature around the semi-sphere Σ, as the function:

$$K(x,y)=\begin{cases}\frac{1}{r^2}, +\sqrt{x^2+y^2+z^2}\le r\\ 0, +\sqrt{x^2+y^2+z^2}>r\end{cases}, \tag{18}$$

Then the Radon transform on the polar disk is:

$$\hat{K}(r,\theta)=\int\limits_{\sqrt{x^2+y^2+z^2}\le r} K(x,y)ds=\frac{1}{r^2}\int\limits_0^r ds=\frac{1}{r}, \tag{19}$$

For other side, the normal curvature of the semi-sphere Σ, comes given by (consider that in the semi-sphere its principal curvatures satisfy $k_1=k_2$), then

$$k(\boldsymbol{u})=k_1\cos^2\theta+k_2\sin^2\theta=\frac{1}{r}=\hat{K}(r,\theta), \tag{20}$$

Furthermore, its normal curvature meets with its mean curvature

$$H=\frac{1}{2\pi}\int\limits_0^{2\pi}k(\theta)d\theta=\left(\frac{k_1+k_2}{2}\right)=\left(\frac{\frac{1}{r}+\frac{1}{r}}{2}\right)=\frac{2}{2r}=\frac{1}{r}, \tag{21}$$

Joining (20) and (21) is proved the lemma.

Then in our real problem we consider the 2-dimensional problem. Then for a 2-dimensional surface in a 3-dimensional space, we have

$$\nabla^2\xi=2\pi\rho, \qquad \xi(x)=k(\boldsymbol{u}),\forall x\in\partial\Omega, \tag{22}$$

which will be the problem with boundary conditions depending of the geometrical enclosure of the sensor for sensing.

Likewise, finally our humidity function considering (9), (16), (17), the conjecture 1. 1, and the lemma 2. 1 will be:

$$\xi(T)=\frac{V\varphi\upsilon}{nRT}\frac{1}{r^2}\left\{\frac{6}{r^4}-\frac{4}{r^2}\right\}e^{k(T-T_0)}, \tag{23}$$

From a topological point of view, the humidity is the action of concentrate the water stem in the air.

We consider the following simple experiment that collect this concentration on a crystal plane (see Figure 4).

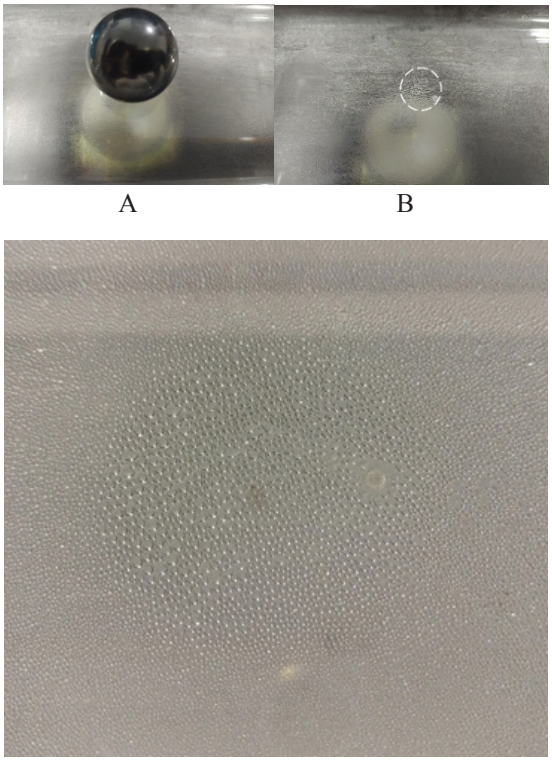

A B C

Figure 4. Experiment that evidences the concentration of water due humidity action.

Then the maximum condensation of humidity will be in a geometrical enclosure region, which we can observe in the figure B, and C, generated by a magnetic sphere on the crystal plane. This proves that the region of sensing of maximum sensing will be in this condensation region. Therefore topologically this has an attribution given by the smooth embedding given for:

$$\sigma:\Sigma\to M^3, \tag{24}$$

where $\sigma(\Sigma)$, is the smooth submanifold embedded smoothly in the space with humidity (air with water).

Likewise, the sensing field whose humidification flow that impact in a surface determines a variation of electrical potential detected by the sensor resistance, which depends on temperature and pressure, this last considering constant (see Figure 5).

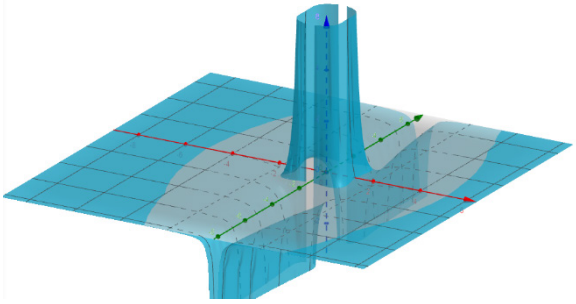

Figure 5. Humidity sensor radial function.

Geometrical enclosure of the sensor for sensing. This surface express the humidity model obtained to curvature energy sensor and proved by the experiment. The surface was done in 3D Geogebra program.

However, the boundary on the sensing region is given by $\xi|_{\partial\Omega} \leq 2\pi\xi(r)$, with $\xi_{ext} = \xi_{\text{int}}$. Their energy require a L^2 – topology [1] defined by a norm or length $\|\xi\|_2$. This norm to measure flow energy will be used to design several sensors and their components to the sensing the humidity of a space and solve of wide form the humidity problem defined.

The radius when $r \to \infty$, then $\xi = 0$. This means that without the dome, the humidity is not sensed. Also, when $r \to 0$, then $\xi \to \infty$, (see the Figure 6). This means that the sensed is the proper resistive element, which senses all humidity element in the pole of the stereographic projection (see Figure 7).

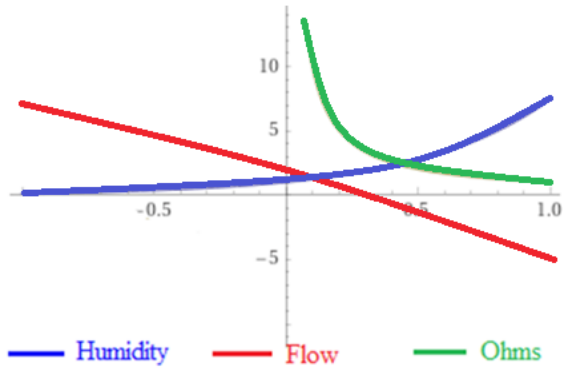

Figure 6. Humidity versus resistance of sensor.

Figure 7. Semi-spherical dome.

3. Minimal Turbulence and Flow Stability

We want to establish a 3-dimensional geometry that does possible the stability of the air dynamics in a determined volume.

The minimal turbulence and air flow stability permits have a volume of static air, optimal condition to measure average temperature and air relative humidity more precise and real (see the Figure 8A, and Figure 8B).

Likewise, and using the curvature energy concept explained in the before section 2, we consider the following design conditions of the sensor:

i) Spherical dome which satisfies all boundary conditions of sensing and permits associate a stereo-radial representation of the signals [9,10].

ii) A minimal hyperboloid permits a coupling of air in its inner cavity and the general medium (see the Figure 5 of humidity sensing surface).

iii) The geometrical element has a direct relation with the harmonicas with the sound phenomenology, criteria based on the musical instruments of air.

The experimental results on the optimality and stability of measurements realized with the sensor with semi-spherical dome are confirmed (see the following experimental sensing graphs (Figures 8A and Figures 8B)). We observe that the sensing with dome coincides or meets with the humidity sensing surface obtained in the Figure 5.

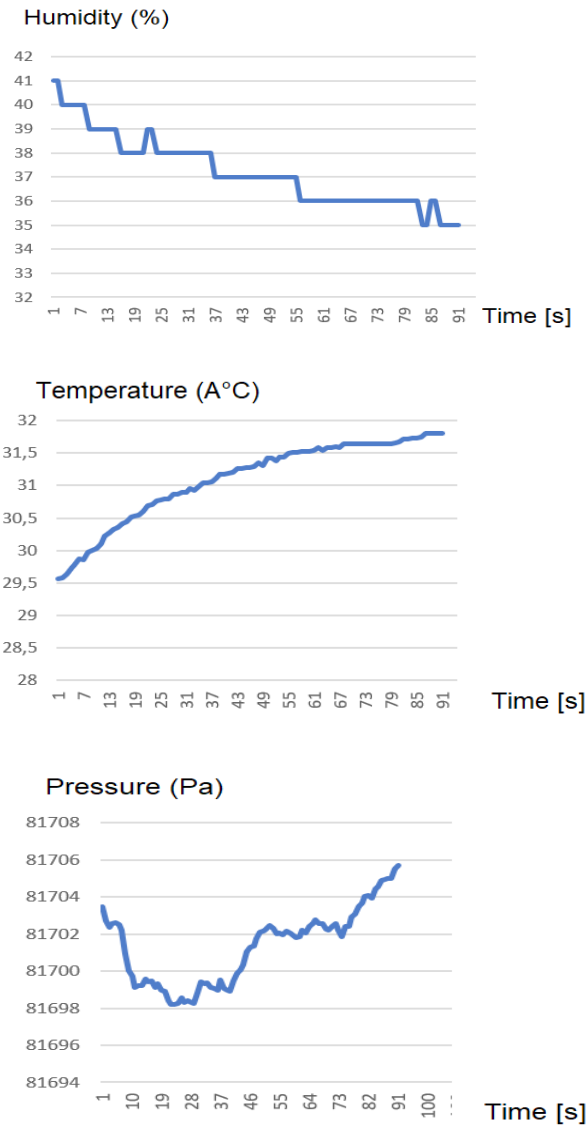

A. Without dome.

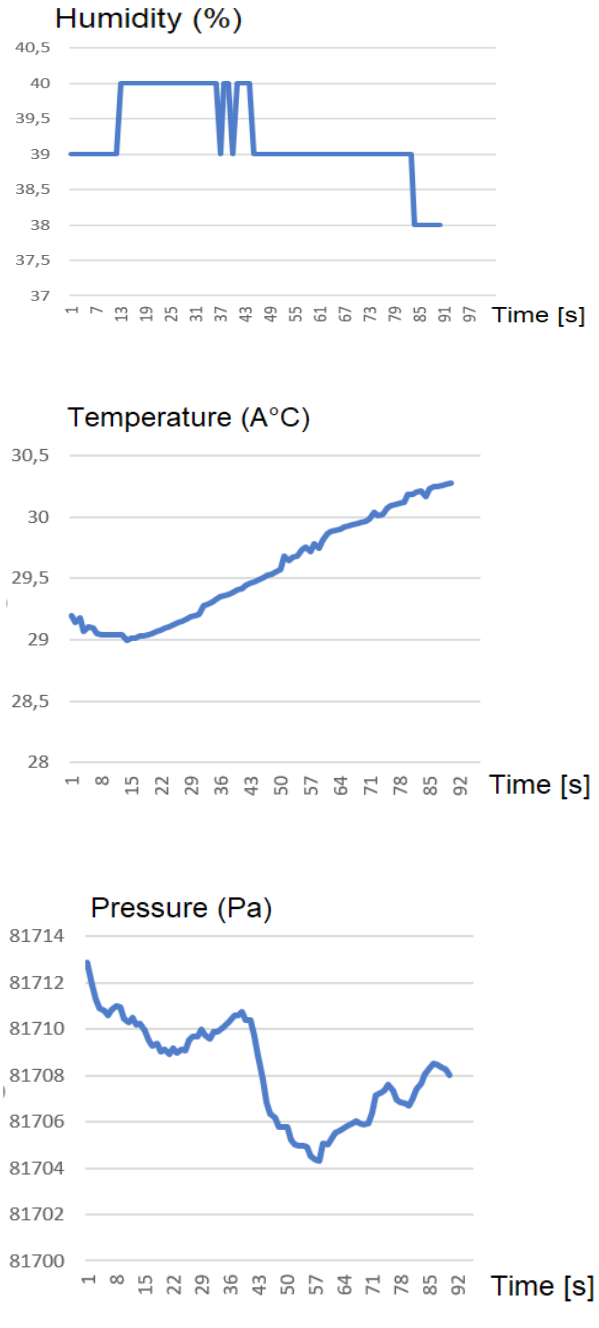

B. With dome.

Figure 8. Measurements realized with the sensor without/ with semi-spherical dome are confirmed.

4. Dynamical System Analysis of Sensor

The sensor device is a semiconductor device of solid state which consists of a resistive element whose interaction with water molecules in the air realizes electrons valence interchange that influence in the change of its electrical resistance (see Figure 9).

Likewise, the alteration of valence internal electrons of the proper semiconductor is realized when varies the temperature influencing in the electrical resistance.

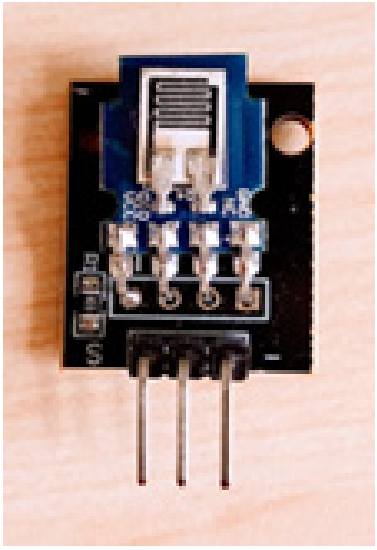

Figure 9. Sensor DTH11. Temperature and humidity sensor with a calibrated digital signal output.

Then we have the scheme:

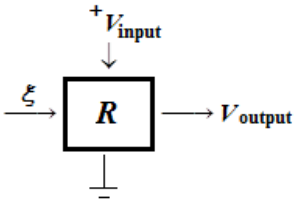

(25)

Then to the dynamics model of the sensor, we consider the fundamental equation:

$$V_s = 5Volts - \xi(T,P)R(t), \qquad (26) \qquad (26)$$

where R, is the resistance of the sensor. Likewise if we consider the potential difference constant then we can have the resistance versus humidity as the curve given by the hyperbole (Figure 10).

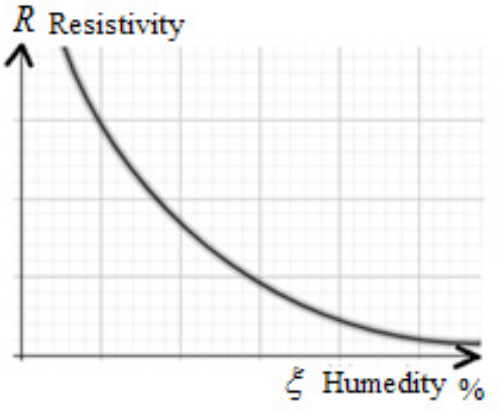

Figure 10. Behavior of the electrical resistance response of the sensor and the humidity variation in the environment.

The humidity signal is $\xi(t) = 60e^{-t/2} + 36$. This comes of the dynamics model of the sensor, and consider the fundamental equation to the model (26).

The resistive element R, is affected for the humidity $\xi(T,P)$, establishing an output voltage, whose difference with the initial voltage (feeding voltage) is directly proportional to the variation of the resistivity affected for the humidity.

The behavior of the electrical resistance response of the sensor and the humidity variation in the environment we can see it in the Figure 10.

The equation (26) implies that $\xi(T,P)$, has units of electric current or its inverse, the admittance. Likewise, there are no indications that there is a direct relationship between ampere [=A] and temperature units [=°C], pressure [=Pa] among others that can affect the phenomenon of humidity in the air.

A new experiment is carried out that consists of the producing an almost the humidity of 95%, a stability time at 95% to the point of going into decline for a time in order to obtain the humidity drop behavior curve and be able to characterize the response curve of the sensor by means of special functions.

Next, the curve that describes the response of humidity expressed in % in the air in a certain time (see Figure 11).

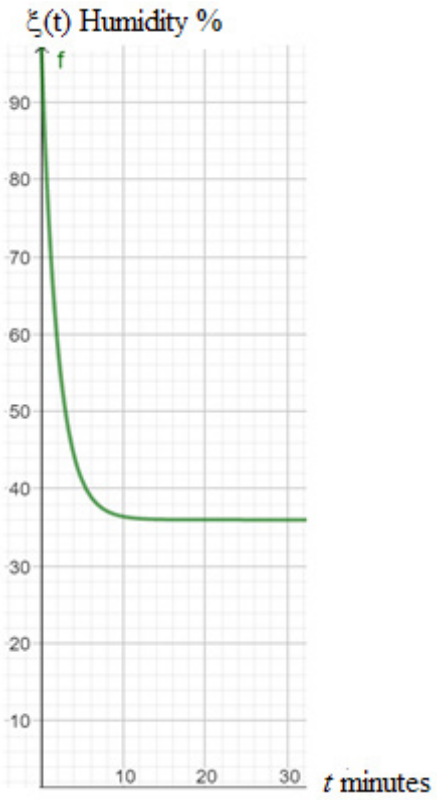

Figure 11. Characterized curve of 95% of humidity until 36% in 9 minutes.

We consider the value of resistance due the humidity as the function $R(\xi)$, where we will assume by separable variables that:

$$R(\xi) = \xi R, \qquad (27) \qquad (27)$$

Then considering the variation with respect to the time, and considering the humidity as function of the pressure and temperature, the Equation (25) takes the form:

$$\xi \frac{dR}{dt} = -\frac{dV}{dt}, \qquad (28)$$

which takes the form considering the Ohm law in the second member[⑤]:

$$\frac{dR}{dt} = -R\frac{V}{\xi L}, \qquad (29)$$

whose general solution is the resistance function:

$$R(t) = \alpha e^{-(V/\xi L)t}, \qquad (30)$$

which includes under measurement conditions the function obtained in laboratory given in the Figure 11. If we consider as initial condition $R(0) = 5volts$, then $\alpha = 5$, then we have the particular law for our sensor:

$$R(t) = 5e^{-(V/\xi L)t}, \qquad (31)$$

Now we want to obtain all dynamical process including the functioning of the sensor in a time interval adding the initial condition and whose enveloping is the function $R(\xi)$, Then we consider the differential equation (29) with the initial condition $R(0) = 5$. Then to a time interval of sensor functioning we have the integral equation of Volterras's type:

$$R(t) = 5 - \frac{V}{L}\int_0^t R(\tau)\xi(x-\tau)d\tau, \qquad (32)$$

where $\xi(t)$, acts as an admittance derived of the proper characteristic as humidity function interacting with the resistive elements justified by the Ohm law.

Likewise realizing the transitory analysis of the system, we have using Laplace transform that:

$$\rho(p) = \frac{5L}{p} - \frac{V}{L}\left[\rho(p)\left\{\frac{60}{p+\frac{1}{2}} + \frac{36}{p}\right\}\right], \qquad (33)$$

whose definition field is the space:

$$\mathsf{D}_{F(p)} = \{p \in \mathsf{C} \,|\, \mathrm{Re}\, p > 0, \mathrm{Re}\, p > -1/2\} \qquad (34)$$

Then applying L^{-1}, to (33) we find that:

⑤Here has been considered an apparent inductor defined by the induction effects that could be established for the inner electrical circuit of the sensor [11,12].

$$R(t)=\frac{5L^2\delta(t)}{96V}-\frac{25e^{-\frac{3}{8}t}}{768V}, \tag{35}$$

which corresponds to the behavior hoped (see experimental graph Figure 12). Here we can consider the value $L=1$, since the inducing factor does not exist as such, however is considered due the effects that could be established for the inner electrical circuit of the sensor.

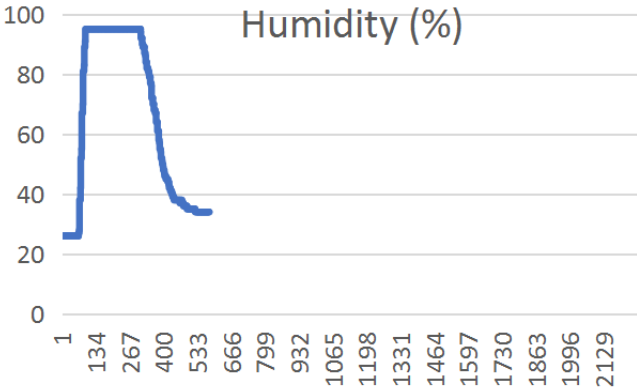

Figure 12. Total nebulizing of humidity with water steam produce the following straight lines and step function. After start decreasing of the humidity in percentage units.

The curvature energy is processed accord to the geometry of the sensor, and the outputs of resistance signals in the sensor involved this curvature energy as can be observed in the solution (35). This only happens in a bandwidth characterized by the average curvature energy

$$\left|\xi\right|_{2,\Omega\partial}\leq\kappa, \tag{36}$$

such and as is established by the Hilbert inequality of the theorem [20]. Then is translated to our spectral problem to [13].

$$\kappa_2\geq H(\omega_1,\omega_2)\geq\kappa_1, \tag{37}$$

where ω_1, and ω_2, are the roots of the polynomial of the energy spectra of the corresponding Jacobi field. Likewise, the design of the sensor with the geometrical enclosure stays finally illustrated in the Figure 13.

The distribution of holes obeys the stereo-radial projection respect to the sensor, and stereographic projection respect any tangent plane $T\Sigma$, to the semi-spherical surface, which does uniform the inputs of air, because their direction is constant of all inputs. The 60 holes have dimensions barely of (0.001984 m) $\approx$ 2 mm of diameter, and the size of holes has been calibrated according to that no influence of the external turbulence.

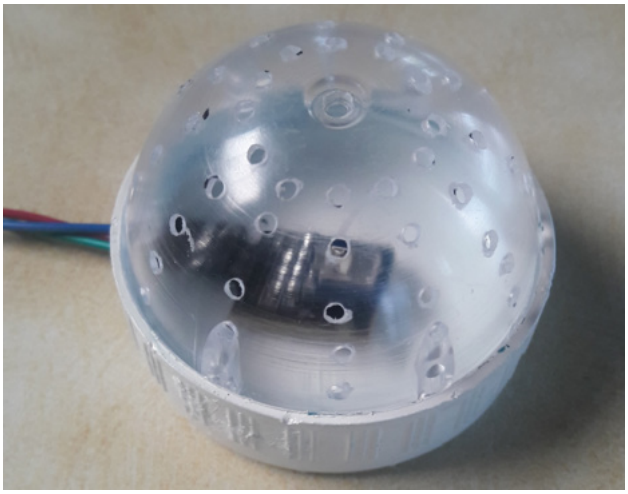

Figure 13. Curvature energy sensor device to humidity obtained.

5. Conclusions

Finally, we can to conclude that we have the possibility to use a conventional sensor to humidity with a special additional geometry to sense the humidity of a 3-dimensional region considering the average curvature energy that can to influence in the good signal reception and sensing process of the humidity under ambient conditions. For the geometrical design was necessary consider the searching of the stability of the air dynamics in a determined volume. The minimal turbulence and air flow stability permits have a volume of static air, optimal condition to measure average temperature and air relative humidity can be more precise and real. Further also, was necessary to consider their cycles in the space where happens this, re-interpreting these cycles from a topological point of view of the current air lines and their transformation in measurable signals as co-cycles where the value of certain integrals on said co-cycles result the sensing data (see the Table 1) useful in the detection and measurement of humidity. Sorting of these data will be obtained a humidity map in real time which can be useful in the study of water and humidity condition in a region of at most 1 kilometer. On the device surface must to exist the boundary condition, $\xi\big|_{\partial\Omega}\leq 2\pi\xi(r)$ to use the curvature energy due the dome geometry whose tangent space defined inside the device establish the addressing of humidity signals for be used in the sensing process. We have the incident humidity flow defined by the tangent space $T_q\Omega$, where in p, is located our resistive sensor.

Table 1. Obtained values during the sensor functioning in a short time interval described in the integral Equation (32) to the description of the dynamical analysis of the system

Time	Started Time(s)	Humidity (%)	Voltage (V)	Temperature(Â°C)	Pressure (Pa)	Altitude(m)
12:57:10	0.00	26	4.76	24.82	80324.17	1916.7
12:57:12	1.00	26	4.77	24.76	80323.6	1916.76
12:57:14	2.00	26	4.77	24.75	80323.21	1916.8
12:57:16	3.00	26	4.76	24.74	80322.5	1916.87
12:57:18	4.00	26	3.78	24.73	80321.8	1916.94
12:57:20	5.00	26	3.7	24.73	80321.43	1916.97
12:57:22	6.00	26	3.7	24.72	80321.4	1916.97
12:57:24	7.00	26	3.7	24.72	80321.36	1916.98
12:57:26	8.00	26	3.7	24.72	80321.03	1917.01
12:57:28	9.00	26	3.7	24.72	80321.17	1917
12:57:30	10.00	26	3.69	24.76	80321.49	1916.97
12:57:32	11.00	26	3.83	24.71	80320.82	1917.03
12:57:34	12.00	26	3.98	24.71	80319.66	1917.15
12:57:36	13.00	26	4.11	24.71	80319.83	1917.13
12:57:38	14.00	26	4.2	24.71	80319.65	1917.15
12:57:40	15.00	26	4.28	24.71	80319.33	1917.18
12:57:42	16.00	26	4.35	24.66	80319.47	1917.17
12:57:44	17.00	26	4.42	24.7	80320.1	1917.11
12:57:46	18.00	26	4.48	24.65	80319.28	1917.19
12:57:48	19.00	26	4.52	24.7	80319.75	1917.14
12:57:50	20.00	26	4.55	24.7	80320.57	1917.06
12:57:52	21.00	26	4.58	24.7	80321.06	1917.01
12:57:54	22.00	26	4.59	24.7	80321.36	1916.98
12:57:57	23.00	26	4.63	24.7	80322.02	1916.91
12:57:59	24.00	26	4.65	24.7	80321.84	1916.93
12:58:01	25.00	26	4.67	24.64	80321.99	1916.92
12:58:03	26.00	26	4.68	24.69	80321.99	1916.92
12:58:05	27.00	26	4.69	24.69	80321.83	1916.93
12:58:07	28.00	26	4.71	24.69	80321.48	1916.97

Conflict of Interest

There is no conflict of interest.

References

[1] Godunov, S.K., 1978. Equations of the Mathematical Physics. Mir Moscow.

[2] Perry, R.H., Green, D.W., 2018. Perry's Chemical Engineers' Handbook (9th Edition). McGraw-Hill, New York, USA, ISBN 0-07-049841-5.

[3] Kobayashi, S., Nomizu, K., 1969. Foundations of Differential Geometry. Interscince Publishers.

[4] Bulnes, F., Martínez, I., Mendoza, A., et al., 2012. Design and Development of an Electronic Sensor to Detect and Measure Curvature of Spaces Using Curvature Energy. Journal of Sensor Technology. 2, 116-126. DOI: http://dx.doi.org/10.4236/jst.2012.23017

[5] Bulnes, F., Martínez, I., Zamudio, O., et al., 2015. Electronic Sensor Prototype to Detect and Measure Curvature Through Their Curvature Energy. Science Journal of Circuits, Systems and Signal Processing. 4(5), 41-54. DOI: https://doi.org/10.11648/j.cssp.20150405.12

[6] Bulnes, F., Martínez, I., Zamudio, O., 2017. Fine Curvature Measurements through Curvature Energy and their Gauging and Sensoring in the Space. Book of Sensors and Applications in Measuring and Automation Control Systems (Advances in Sensors: Reviews, Vol 4, Chapter 20, (Ed.) Sergey Y. Yurish, IFSA Publishimg, Barcelona, Spain (2017).

[7] Wiederhold, P.R., 1997. Water Vapor Measurement, Methods and Instrumentation. Marcel Dekker, New York, NY ISBN 9780824793197.

[8] Bulnes, F., 2001. Radon Transform and Curvature of an Universe. UNAM Postgraduate Thesis.

[9] Wilczynski, E.J., 1904. Projective Differential Geometry of Curves and Ruled Surfaces. Leipzig B.G. Teubner.

[10] Kobayashi, W., Horst, S., 1983. Topics in Complex Differential Geometry Function Theory on Noncompact Kähler Manifolds. Birkhäuser Basel.

[11] Salam, M.A., Rahman, Q.M., 2018. Fundamentals of Electrical Circuit Analysis. Springer.

[12] Tietze, U., Schenk, C., Gamm, E., 2015. Electronics Circuits: Handbook for Design and Applications, Springer.

[13] Hsu, H.P., 1984. Applied Fourier Analysis. Books for Professionals Collection.

BILINGUAL PUBLISHING CO.
Pioneer of Global Academics Since 1984

Electrical Science & Engineering
https://ojs.bilpublishing.com/index.php/ese

ARTICLE

Overview of Key Technologies for Water-based Automatic Security Marking Platform

Aijuan Li[1*] Chunpeng Gong[1] Xin Huang[2] Xinnian Sun[3] Gang Liu[4]

1. School of Automotive Engineering, Shandong Jiaotong University, Jinan, Shandong, 250357, China
2. School of Information Science and Electrical Engineering, Shandong Jiaotong University, Jinan, Shandong, 250357, China
3. Research and Development Center, Hangzhou Jiahe Electric Co., Ltd, Hangzhou, Zhejiang, 310053, China
4. Labor Union, Shandong Jiaotong University, Jinan, Shandong, 250357, China

ARTICLE INFO

Article history
Received: 11 May 2022
Revised: 03 June 2022
Accepted: 07 June 2022
Published Online: 15 June 2022

Keywords:
AUV
ROV
USV
Information fusion
Underwater security screening

ABSTRACT

Water-based automatic security marking platform composed of multifunctional underwater robots and unmanned surface vessel has become the development trend and focus for exploring complex and dangerous waters, and its related technologies have flourished and gradually developed from single control to multi-platform collaborative direction in complex and dangerous waters to reduce casualties. This paper composes and analyzes the key technologies of the water-based automatic security marking platform based on the cable underwater robot and the unmanned surface vessel, describes the research and application status of the key technologies of the water-based automatic security marking platform from the aspects of the unmanned surface vessel, underwater robot and underwater multi-sensor information fusion, and outlooks the research direction and focus of the water automatic security inspection and marking platform.

1. Introduction

The underwater environment is complex, human diving depth is limited and dangerous, and water safety is an important task for public security organs. For underwater detection, search, detonation, and other work, frogmen are primarily used for manual processing, which not only makes the case inefficient but also poses a risk to personnel safety. Underwater robots can replace divers for underwater work in complex and risky conditions. Robots are also fast-growing and becoming widely employed in numerous industries, thanks to the Internet of Things,

*Corresponding Author:
Aijuan Li,
School of Automotive Engineering, Shandong Jiaotong University, Jinan, Shandong, 250357, China;
Email: liaijuan@sdjtu.edu.cn

DOI: https://doi.org/10.30564/ese.v4i1.4710

big data, cloud computing, artificial intelligence, and other high-tech. The underwater environment is complex, human diving depth is limited and dangerous, and water safety is an important task for public security organs. For underwater detection, search, detonation, and other work, frogmen are primarily used for manual processing, which not only makes the case inefficient but also poses a risk to personnel safety. Underwater robots can replace divers for underwater work in complex and risky conditions. Robots are also fast-growing and becoming widely employed in numerous industries, thanks to the Internet of Things, big data, cloud computing, artificial intelligence, and other high-tech. Police robots can not only assist the police in completing some daily tasks for the public's convenience but also in a variety of security activities to replace police patrol work and reduce police casualties [1]. They can also replace the police in toxic and hazardous work in reconnaissance, detonation, rescue, and other tasks to reduce police casualties. The deployment of robots in dangerous areas is critical for reducing fatalities.

The underwater fully automated security check marker platform is a heterogeneous platform system based on Unmanned Surface Vessel (USV) and Remotely Operated Vehicle (ROV), as shown in Figure 1. Underwater robots require positioning services from a mother ship when performing underwater operation tasks, which limits the range of activities of underwater robots [2]. Replacing the mother ship of the underwater robot with a USV can be used as a relay station to provide energy resupply and information interaction for the underwater robot, forming a heterogeneous robotic synergy platform between the USV and the underwater robot to improve the operational efficiency of the underwater robot and reduce costs [3]. In addition, there are many research institutions that collaborate USVs with underwater robots or other devices [4]. The literature [5] proposed the synergistic operation of USVs with unmanned aerial vehicles (UAVs) to enhance the advantages of USVs and UAVs and form a new collaborative platform of coupled USV-UAV systems. The literature [6] investigates the design, construction and control strategies of USV-ROV systems with the aim of developing inspection and surveillance technologies that are compatible with maritime and submarine applications. The literature [7] presents the development of the USV-ROV maritime unmanned platform architecture, control system, sensor system and control algorithms, as well as the results of sea trials.

The water-based automatic security marking platform consists of USV, ROV, water control system, launch and recovery system, umbilical cable, cable management system and other devices, as shown in Figure 2 [9]. The water-based fully automated security marking platform incorporates a number of advanced technologies such as sensor technology, wireless communication technology, data processing technology, and intelligent control technology [10]. The USV, for example, is designed like a double-hulled surface boat and has superb speed, wave resistance, maneuverability, and stability [11]. The use of air channels to generate surface power, along with an air culvert power system on the water, can prevent interference and encroachment on the hydrographic situation and the equipment carried on the hull caused by the undersea rudder and propeller propulsion system. The use of air channels to generate surface power, along with an air culvert power system on the water, can prevent subsea rudder and propeller propulsion system interference and encroachment on the hydrographic situation and the equipment carried on the hull. The underwater robot is launched and recovered by the launch and recovery system, and the length of the loaded umbilical cable is proportional to the robot's diving depth. The cable management system is a two-strand cable-connected housing intermediary device that can be used to store and stow the neutral cable, minimize or lessen the effect of the surface mothership's motion on the ROV, and increase the underwater robot's operational radius. The umbilical cable transmits both power and control signals from the unmanned surface boat to the underwater robot in the forward direction and image data from the underwater robot to the unmanned surface boat in the reverse direction in real-time, mainly involving information transmission technology [12]. The water-based automatic security marking platform is equipped with a high-precision sonar detector, by wireless operation platform for underwater structure modeling, hull connection control multifunctional underwater robot, the robot equipped with underwater high-definition camera set, high-power searchlight, metal detector, node detector, capable of information fusion processing, integrated sonar and electromagnetic detection function, sonar detection accuracy of different water quality research, the use of electromagnetic detection to determine the type of target object, able to study and judge the high-risk area and issue an alarm, the hull to mark the dangerous area, mainly involving sonar detection, multi-sensor information fusion and other technologies.

This study focuses on the essential technologies used in completely automated security marking platforms on water, such as unmanned surface vehicles, multifunctional underwater robots, multi-sensor fusion detection, and so on, and forecasts the trend of fully automated security

screening platforms on water.

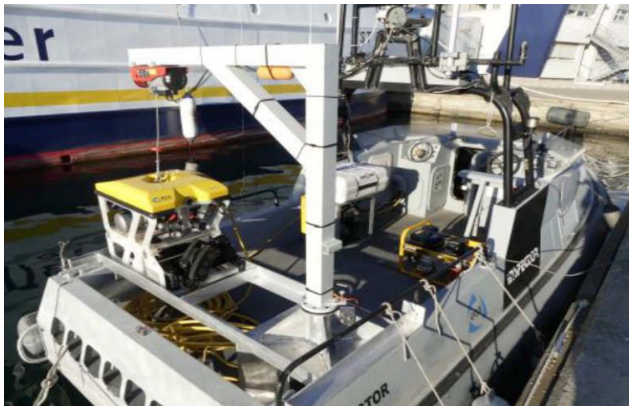

Figure 1. USV-ROV [8]

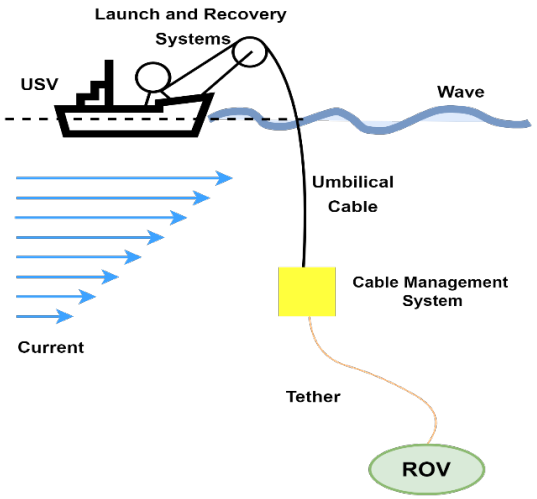

Figure 2. Structural components of the water automatic security check marker platform [9]

2. Water-based Automatic Security Marking Platform Key Technology Research Status

2.1 Research on USV

USVs are classified as propeller or water jet propulsion based on their propulsion method [13]. USVs are fitted with advanced control systems, sensor systems, and communication systems to undertake a variety of complicated missions such as scientific research, environmental missions, maritime resource exploitation, military use, detection, and hazardous missions such as demining. Figure 3 depicts a description of the challenge, research issues, and current state of the art for USVs.

USVs were first developed during World War II and were primarily employed for military purposes [14]. USVs were widely deployed in the US Army's anti-mine ship system in the 1970s and played a key part in military missions [15]. The USV is an open architecture design with a range of mission-oriented modular components developed by Textron [16]. The Watcher II, built by Yunzhou Technology Co., Ltd. in China, is the world's second unmanned missile boat and one of only two unmanned missile boats to successfully execute missile test firings [17]. The USV features a number of different piloting modes. The USV has numerous piloting modes and is outfitted with electro-optical and radar equipment as well as missile launchers, allowing it to conduct intelligent patrol, reconnaissance, and search and rescue operations.

USV has also been applied in post-disaster search operations and structural damage assessment, such as the World Trade Center in 2001, Fukushima Daiichi nuclear power plant in 2011, Hurricane Wilma in 2005 and Hurricane Ike in 2008 [18]. The literature [19] summarized and prospected the application and role of USV in disaster relief to provide some theoretical guidance for the research in this field. Scientific research is another need for USVs, with experts from C & C Technologies and Texas A & M University employing them for hydrographic surveys and scientific applications [20]. The China Meteorological Administration (CMA) built the "Tianxiang *I*" in 2008, which was the first international usage of autonomous marine exploration vessels for meteorological exploration. The "*Jinghai*" series of surface unmanned boats, developed by Shanghai University, can detect underwater topography and hydrology, as shown in Figure 4. It has also conducted polar marine mapping in Antarctica, making it China's first unmanned surface vessel to do independent mapping in the polar areas [21]. Literature [22] proposed that an autonomous boat that uses waves as propulsion and solar panels to power electronic equipment attain extraordinarily long endurance and play a key role in encouraging the implementation of worldwide ocean observation expeditions.

Underwater robots must be deployed and recovered regularly due to their range and the stability of underwater data transmission. This raises the expense and risk, as well as the inability to operate 24 hours a day, seven days a week, and with low efficiency. As a result, using unmanned surface boats to boost underwater robot performance has a lot of practical applications. The underwater automatic security check marker platform employs cable remote control of the underwater robot, as well as cable remote control of the underwater robot and unmanned surface boat via umbilical cable connection, with umbilical cable forward transmission of power and control signals from the unmanned surface boat to the underwater robot, as well as reverse real-time image data transmission from the underwater robot to the unmanned surface boat. Some ROVs with sufficiently strong armored or umbilical

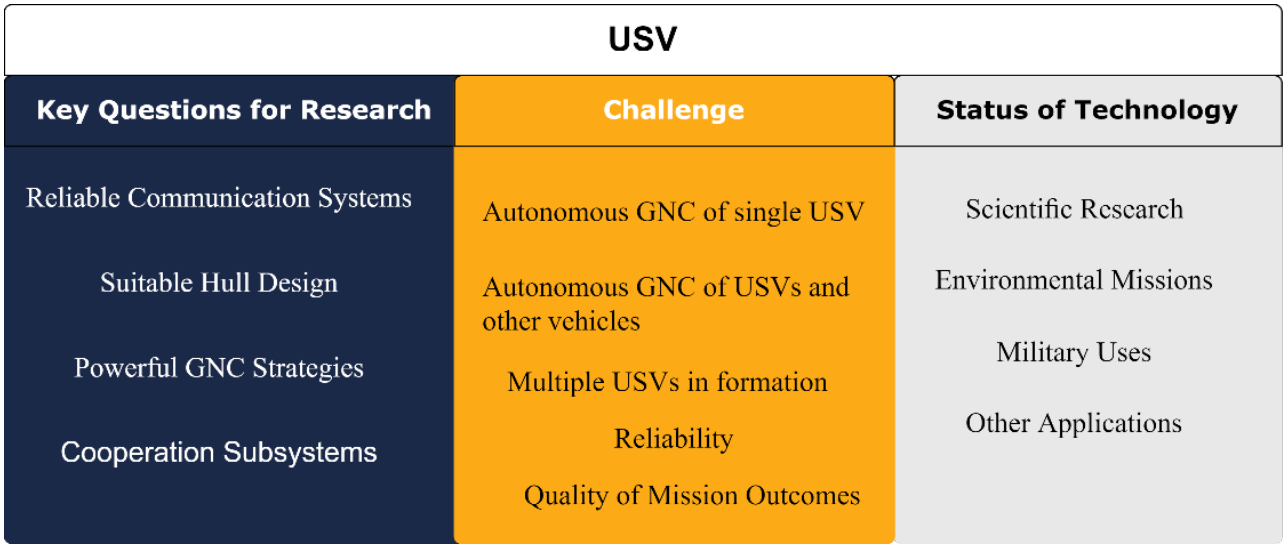

Figure 3. The summary of the current status of USV research

cables can rely on the armored or umbilical cables to pull the ROV body out of the water if the body loses power in the event of failure. ROVs have substantially improved in terms of safety [23].

In conclusion, USVs are becoming more common in scientific studies and some maritime operations. The deployment of USVs can significantly enhance work efficiency, minimize people activities above and below the sea, and lower hazards and expenses. The potential of USVs for marine scientific research and military applications is clear, including the junction of numerous disciplines, particularly in the realm of artificial intelligence, and the future development trend is for USVs to be extremely intelligent. A current research focus is how to increase the autonomous capabilities of unmanned surface boats in order to complete various tasks in challenging operational settings. To make the intelligent system more forward-looking, unmanned surfaces improve the capacity to forecast the future and boost the system's autonomous learning capabilities.

Figure 4. *"JingHai-I"* USV [24]

2.2 Research on Underwater Robots

Underwater robots are a form of extreme operating robot that works underwater. They come in a variety of shapes and sizes and have been in development for over 60 years [25]. Depending on whether there is an umbilical cable between the mother ship and the hull, unmanned underwater robots are classified as Remotely Operated Vehicles (ROV) or Autonomous Underwater Vehicle (AUV). In real-time, the umbilical cable transfers power and control signals from the mother ship to the vessel in one direction and picture data from the vessel to the mother ship in the other. The AUV, on the other hand, has no umbilical cord connecting it to the mother ship; instead, it navigates autonomously using the power source integrated into the hull and its intelligence. The umbilical cable provides power, information exchange, and safety for ROVs, but it also limits the range of activities that ROVs can perform. As a result, AUVs, which do not require umbilical cables, are self-energizing, and operate on autonomous forces, have naturally become a hot spot for research. However, there are significant technological challenges in building AUVs, and the technology is not yet mature. Figure 5 depicts a description of the challenge, research issues, and current state of the art in the field of underwater robots.

2.2.1 AUV

In comparison to ROVs, AUVs do not require umbilical cords to link to the mother ship and hence have a larger operating radius, more maneuvering freedom, smaller size, and no requirement for expensive life support and surface support systems [26]. Because of their distinct advantages,

Underwater Robotics			
	Key Questions for Research	**Challenge**	**Status of Technology**
ROV	**Seafloor Topography** **Top-flow anti-interference capability** **Detection and Identification of Underwater Targets**	**Operating Accuracy** **Range of Activities** **Hydraulic Power**	**Mature Technology** **Reach Almost Any Ocean Depth** **Wide range of applications**
AUV	**Dynamics of AUV** **Multi-AUV Communication Technology** **Navigation Positioning** **Control Technology**	**Adequate Power Supply** **AUV Docking Technologies** **Information Transmission** **Submergence depth**	**Research Hotspots** **Excellent Potential Applications** **Technology is Still Immature**

Figure 5. The summary of the current status of Underwater Robots research

AUVs are used in a variety of industries, including military, civilian, and scientific research. AUVs are mostly utilized for underwater construction, patrol and reconnaissance, and intelligence gathering in the military, which is why governments all over the world are working to develop better AUV systems [27]. Advanced AUV systems have been developed around the world. The US military uses the REMUS line of underwater robots created by Woods Hole Ocean Systems Laboratory for military operations such as mine countermeasures [28]. The United States deployed the REMUS series of underwater robots developed by Woods Hole Ocean Systems Laboratory in military duties such as anti-mine operations [29]. REMUS-6000 and other autonomous underwater robots were later developed for underwater searches and mapping [30]. AUVs are extensively utilized in the civilian sector for maritime rescue, submarine fiber optic cable laying, maintenance, and other tasks. In 2014, the Zhejiang Hangzhou Public Security Bureau used an underwater robot to recover a murdered person's body from a reservoir with a water depth of over 100 meters. The civilian police were aided by the Wuhan Public Security Bureau's multifunctional detonation robot in safely and efficiently accomplishing rescue and detonation tasks in tough conditions. This will considerably lower the risk of work and the number of civilian police officers killed. Underwater robots are mostly utilized in scientific study for topographic mapping, seabed mineral exploration, marine environmental studies, and marine archaeology, among other things. The "*Qianlong*" series includes two underwater robots, "*Qianlong I*" and "*Qianlong II*" which were produced by China for oceanographic study. The "*Qianlong I*" can work at a maximum depth of 6000 meters. It has a shallow stratigraphic profiler and other exploration equipment, as illustrated in Figure 6 [31], enabling fine exploration of seabed microtopography and geomorphology, as well as monitoring of seafloor hydrographic parameters. The greatest dive depth of Harbin Engineering University's "*Wukong*" reached 7709 meters in 2021, setting a new record for unmanned cableless submersible AUV dive depth and making it the second deepest in the world [32]. This is the world's second-deepest AUV.

Because there is no impact of cable and limited fluctuation in sea state parameters, AUV has significant benefits in operational capability and precision. As a result, AUV will be one of the future trends of underwater multipurpose robots with outstanding prospective application possibilities. Multi-autonomous underwater vehicle (Multi-AUV) underwater cooperative operation is now the trend and focus of underwater robot research, and because the underwater environment is complicated and changing, multi-AUV formation can better accomplish diverse duties. The literature [34] suggested an integrated algorithm for cooperative operation of Multi-AUV, which enhances search

efficiency and decreases tracking mistakes while maintaining high efficiency and flexibility. The literature [35] evaluated the impacts of the AUV model, underwater environment, and intra-AUV communication on formation transformation and recommended several difficult difficulties and future research paths for Multi-AUV formations.

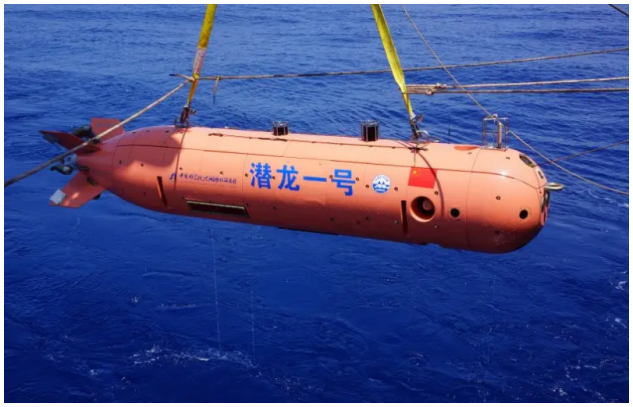

Figure 6. "*Qianlong I*" AUV [33]

2.2.2 ROV

ROV technology is the most advanced and widely utilized, with operating depths ranging from 0 to 10,000 meters and the ability to reach nearly any ocean depth. The ROV is connected by cable to the mother ship, which supplies power, energy, data transmission, and control. As demonstrated in Figure 7, ROV has better data transmission and range than AUV and is not limited by the ocean environment, making it appropriate for substituting people in a variety of industries to complete some dangerous duties. Japan's "Trench" ROV and the U.S. "Poseidon" ROV have reached the deepest place on Earth - the Marianas Trench. In 1985, China's first large underwater robot, the Sea Man One ROV, was developed to conduct scientific research. ROVs can also be utilized in police applications such as underwater suspicious object detection and rescue, underwater security, and underwater disposal, and can replace frogmen in risky, sensitive, or long and repetitive labor. The literature [36] uses ROVs for underwater inspection of ship hulls or marine debris, etc., equipped with cameras and sensors such as GPS, temperature, depth and pressure to achieve protection of the marine environment as well as underwater species. ROVs are used to do maintenance inspections of coastal berms or coastal buildings, according to the literature [37]. Virtual reality (VR) technology is used in the literature [38] to remotely operate ROVs, which can let users feel as if they are in a risky scenario without having to be physically present. ROV sensor data is converted into human-perceivable experiences using a VR sensory simulator. The hurdles to person-in-the-loop ROV teleoperation are reduced by allowing substantial human engagement in ROV teleoperation.

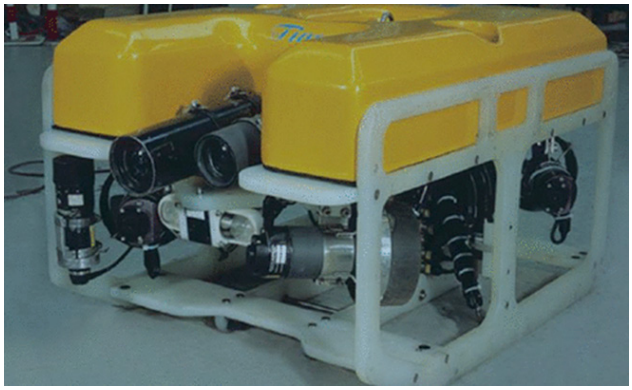

Figure 7. ROV [39]

There is still more opportunity for AUV development than ROV due to the limits of related technology development levels [40]. The ROV system is the most established, frequently utilized, cost-effective, and practical submersible [41]. ROVs are classified as observation or operational, and the water-based automatic security marking platform uses an observation level ROV with underwater thrusters and underwater camera systems as its core components, which are sometimes supplemented by navigation, depth sensors, and other conventional sensors.

The ROV body is smaller, lighter, and carries a reduced burden. One of the trends in the development of ROVs is improving the operational synergy between the surface control system and the underwater observation operation system, increasing data processing capability and speed, and improving the overall ROV operational control level and operational performance [42]. ROVs use umbilical cords to provide data, control commands, and energy to the surface platform. The length of the loaded umbilical cable is proportional to the underwater robot's dive depth and operational radius, which is overly reliant on the surface USV, resulting in a limited range of activities and a dive depth that has to be enhanced. The umbilical cable has a particular rigidity and buoyancy, and its contact with the ROV can impact the underwater robot's operational precision to some amount. As a result, one of the most important research concerns in the future will be decreasing the cable's impact on the underwater robot or creating AUV technology. The combination of AUV and ROV to form a water-based automatic security marking platform is an important development direction and hot spot for future safety in complex waters, and they both play their respective irreplaceable roles in complex waters considered for detection, complementing the characteristics of AUV and ROV to improve the efficiency of underwater operations.

2.3 Research on Underwater Multi-sensor Information Fusion

Because the underwater environment is complicated and varied, individual sensors are less dependable, hence underwater data fusion is critical. The correlation and fusion of information and data acquired by each sensor in time and space to remove redundant information and produce a consistent interpretation and description of the observed object so that the obtained information is fully utilized are referred to as multi-sensor information fusion. Fusion can be classified into three types based on the structure of the data: data-level fusion, feature-level fusion, and decision-level fusion [24]. A summary of USV challenges, research issues, and the current state of the art is presented in Figure 8.

The literature [43] designed a submarine pipeline detection method based on multi-sensor information fusion, capable of collecting acoustic profiles and topography above and below the water in the area of the pipeline route. Inspection of underwater infrastructure, such as bridges, water supply systems and oil rigs, requires divers to be in the water to perform the task. Because underwater habitats are complicated and all environments are unknown and harmful to divers, the employment of underwater robots to create maps of the environment and locate them can lessen the risk to divers. The literature [44] combined vision, inertial, acoustic and pressure sensors using SLAM algorithm to achieve simultaneous localization and mapping in underwater environment. In the literature [45], data fusion using sensors such as IMU, pressure and optical flow was used to achieve underwater centimeter-level localization using an extended Kalman filter fusion algorithm to improve localization accuracy and achieve optimal navigation [46]. This underwater robot localization method with a modest processing capacity is useful for operational duties in unfamiliar underwater environments. Because GPS is no longer applicable in unknown complex underwater environments, which is extremely dangerous for divers, it is necessary to use underwater robotic detection and real-time map construction, i.e. positioning, as well as to quickly correct the course at any time based on changes in motion sensors and navigation parameters. Although the present multi-sensor data fusion detection technology is advanced, its use in the underwater environment is still uncommon. Some essential technologies, including as high-level representations of data fusion, target tracking identification, and its fusion algorithms, still require improvement [47].

The lowest level of fusion is data-level fusion, which is the direct data fusion of the raw data obtained by each sensor for the detection target, without any pre-processing [48]. As demonstrated in Figure 9, data-level fusion is commonly employed for data fusion of the same type of sensor [49].

Pre-processing the original information obtained by each sensor first, extracting representative features in the information for feature fusion, and then performing target recognition based on the fused features is what feature-level fusion is all about. This fusion method preprocesses the original data and eliminates redundant data, which improves the sensing system's real-time performance. However, as illustrated in Figure 10, certain critical information may be lost in the preprocessing, resulting in perception system misjudgment.

As shown in Figure 10, decision-level fusion is a high-level fusion that complements (integrates) data-level and feature-level fusion. To accomplish optimal target detection, each sensor first detects the target to obtain its judgment results, and then these decisions are correlated and integrated, as illustrated in Figure 11. Decision-level fusion can make the best use of the data collected, but it requires a lot of processing power. The literature [50] proposed the use of Bayesian fusion method for underwater

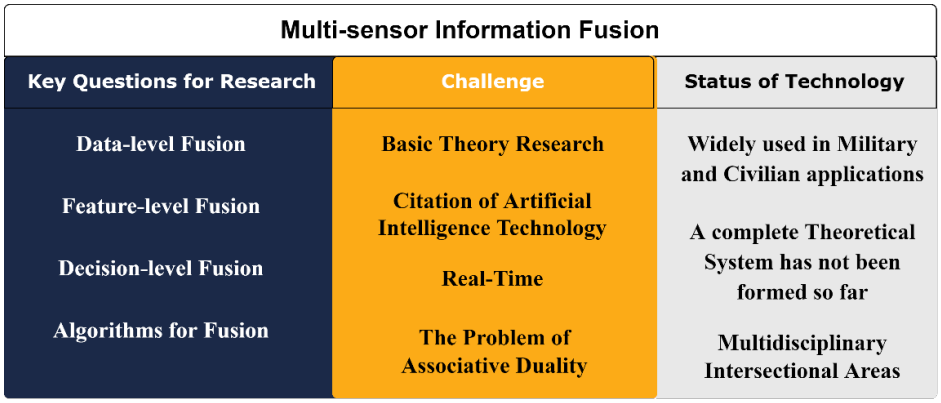

Figure 8. The summary of the current status of Multi-sensor Information Fusion research

multi-sensor information fusion, where each sensor makes a decision before submitting it to the fusion center to make the final decision, this fusion reduces the data transmitted by the underwater robot like the data center, reduces the computational complexity of the fusion middle row, and facilitates the underwater transmission.

The multi-functional underwater robot uses a decision fusion mechanism to judge and make decisions on targets by integrating multiple sensors such as sonar, electromagnetic detection, and high-definition cameras and then passing the results of the decisions to the fusion center, where they are fused. The accuracy of sonar detection of various water quality, the use of electromagnetic detection to determine the type of target, the capacity to study and judge high-risk zones and send alerts, and the use of the hull to indicate the danger area are all investigated. Because the extracted features are directly related to the decision analysis, the fusion results can maximize the feature information required for decision analysis, considerably boosting the system's efficiency. However, each sensor in this distributed fusion process determines only its data information, and the correlation between data is not taken into account [51]. The data correlation isn't properly taken into account.

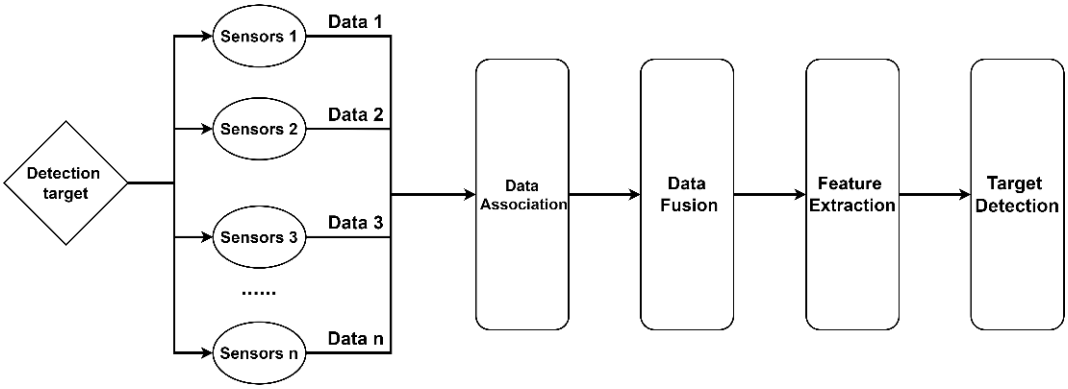

Figure 9. Data-Level Fusion

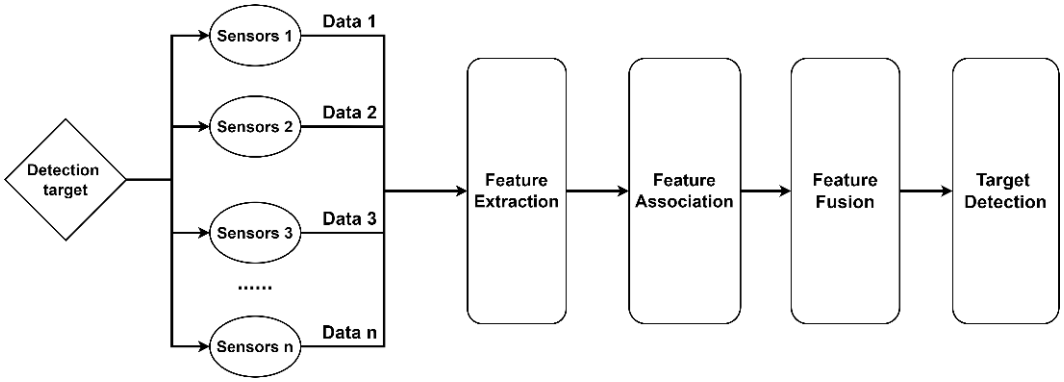

Figure 10. Feature-Level Fusion

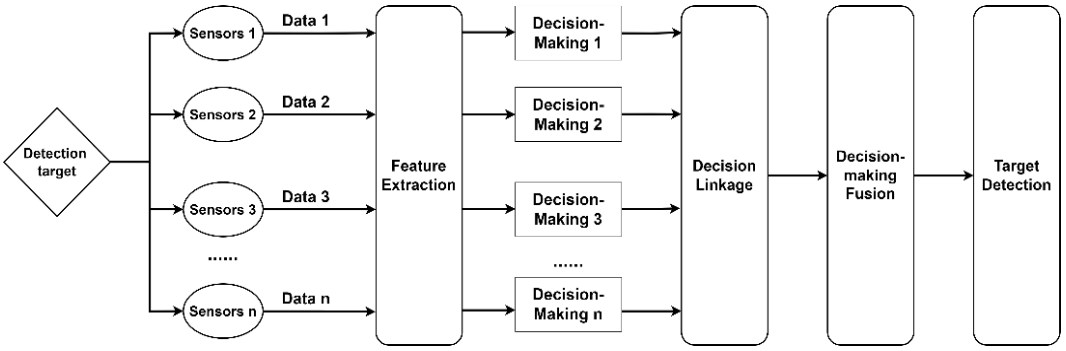

Figure 11. Decision-Level Fusion

3. Conclusions

The water-based automatic security marking platform by integrating a range of systems, such as ROV, USV, and surface control and launch recovery system, to achieve high-risk area research and marking. To prevent civilian casualties, the creation of a fully automatic security inspection platform on the water could replace civilian police in poisonous and hazardous operations such as reconnaissance, detonation, rescue, and other jobs. Underwater and surface control command and data transfer, underwater robot range and operating capabilities, high-precision motion control capability, environment perception capability, and positioning capability are the important technologies. The underwater robot is a critical component of the water-based automatic security marking platform on the sea, offering substantial mobility, flexibility, and endurance. Underwater robots combine modern technologies in mechanics, materials, energy, fluids, computer control, and other domains. Underwater multifunctional robotics development is critical for military, civic, and scientific study. This paper researches and summarizes the key technologies involved in the water-based fully automated security marking platform, which provides a certain reference for the research in the field of water safety and is of great significance for reducing casualties.

Despite the fact that research on the USV-ROV collaborative system is growing, it still has significant issues to address due to the unique nature of its working environment and application context. Satellite communication currently covers practically the whole globe, however it cannot be utilized underwater. One of the most important components of a USV-ROV utilized for underwater operations is the communication system, which increases underwater communication performance in three ways: efficiency, dependability, and safety. The water-based fully automated security marking platform should be able to make intelligent autonomous decisions in a tough environment. In the event of a communication failure, it may self-adopt a series of coping mechanisms to establish autonomous route planning and control capacity for underwater operations.

Acknowledgments

This project is supported by National Natural Science Foundation of China (Grant No. 51505258 and 61601265), Natural Science Foundation of Shandong Province, China (Grant No. ZR2015EL019, ZR2020ME126 and ZR2021MF131), The Youth Science and Technology Plan Project of Colleges and Universities in Shandong Province (Grant No. 2019KJB019), Open project of State Key Laboratory of Mechanical Behavior and System Safety of Traffic Engineering Structures, China (Grant No. 1903), Open project of Hebei Traffic Safety and Control Key Laboratory, China (Grant No. JTKY2019002).

Conflict of Interest

There is no conflict of interest.

References

[1] Chen, D.J., 2020. Research on the status of application of police robots in Zhejiang public security. Light Industry Science and Technology. 36(05), 69-71.

[2] Hui, X.U, Jiang, C., 2021. Heterogeneous oceanographic exploration system based on USV and AUV: A survey of developments and challenges.

[3] German, C.R., Jakuba, M.V., Kinsey, J.C., et al., 2012. A long term vision for long-range ship-free deep ocean operations: Persistent presence through coordination of autonomous surface vehicles and autonomous underwater vehicles. 2012 IEEE/OES Autonomous Underwater Vehicles (AUV). IEEE. pp. 1-7.

[4] Liu, Y., Liu, W., Song, R., et al., 2017. Predictive navigation of unmanned surface vehicles in a dynamic maritime environment when using the fast marching method. International Journal of Adaptive Control and Signal Processing. 31(4), 464-488.

[5] Shao, G., Ma, Y., Malekian, R., et al., 2019. A novel cooperative platform design for coupled USV–UAV systems. IEEE Transactions on Industrial Informatics. 15(9), 4913-4922.

[6] Nava-Balanzar, L., Sánchez-Gaytán, J.L., Fonseca-Navarro, F., et al., 2017. Towards Teleoperation and Automatic Control Features of an Unmanned Surface Vessel-ROV System: Preliminary Results. ICINCO (2). pp. 292-299.

[7] Lee, J., Jin, H.S., Cho, H., et al., 2020. A New Complex Marine Unmanned Platform and Field Test. Journal of Marine Science and Technology. 28(6), 9.

[8] Lachaud, E., Monbeig, Y., Nolleau, P., et al., 2018. Opportunities and Challenges of Remote Operating a ROV Embarked on a USV. Offshore Technology Conference. OnePetro.

[9] Quan, W., Liu, Y., Zhang, A., et al., 2016. The nonlinear finite element modeling and performance analysis of the passive heave compensation system for the deep-sea tethered ROVs. Ocean Engineering. 127, 246-257.

[10] Chen, Z.H., Sheng, Y., Tao, J., 2009. A review on the

structure of remotely operated underwater robots-Example of HYSUB130-4000 ROV system. Marine Geology. 3, 64-71.

[11] Liu, Q., Tan, Y.X., 1999. Research on the difference between single and catamaran taxi boats and the scope of application of catamaran taxi boats. Jiangsu Ship. (02), 33-36+44.

[12] Wu, J., Wang, Z.D., Ling, H.J., et al., 2020. Review of key technologies for deep-sea operational underwater robots with cables. Journal of Jiangsu University of Science and Technology (Natural Science Edition). 34(04), 1-12.

[13] Barrera, C., Padron, I., Luis, F.S., et al., 2021. Trends and challenges in unmanned surface vehicles (Usv): From survey to shipping. TransNav: International Journal on Marine Navigation and Safety of Sea Transportation. 15.

[14] Corfield, S., Young, J., 2006. Unmanned surface vehicles-game changing technology for naval operations. IEEE Control Engineering Series. 69, 311.

[15] Tang, H.B., 2020. Research status and development trend of surface unmanned boats. Ship Materials and Markets. (03), 13-14.

[16] He, P., Yang, M., Ma, Y., 2012. Global naval warfare robot. Beijing PLA Press.

[17] Liu, J.P., 2019. Unveiling the prologue of unmanned naval warfare, China's "Lookout" II unmanned boat. Tank Armored Vehicle. (02), 26-30.

[18] Moud, H.I., Shojaei, A., Flood, I., 2018. Current and future applications of unmanned surface, underwater, and ground vehicles in construction. Proceedings of the Construction Research Congress. pp. 106-115.

[19] Jorge, V.A.M., Granada, R., Maidana, R.G., et al., 2019. A survey on unmanned surface vehicles for disaster robotics: Main challenges and directions. Sensors. 19(3), 702.

[20] Sager, W.W., Shyu, J.P., Manley, J., 2008. Exploring West Florida Escarpment with High-Resolution Geophysical Imaging. UNE. 1, 11.

[21] Peng, Y., Luo, A.X., 2015. The battle at sea-A chronicle of Shanghai University's Jinghai unmanned boat series development. China Military to Civilian. (02), 37-39.

[22] Hine, R., McGillivary, P., 2007. Wave powered autonomous surface vessels as components of ocean observing systems. Proceeding of PACON. pp. 1-9.

[23] Song, Zh.W., 2016. Underwater structure inspection and operation robot ROV development and sonar image recognition research. Jiangsu University of Science and Technology.

[24] Peng, Y., Yang, Y., Cui, J., et al., 2017. Development of the USV "JingHai-I" and sea trials in the Southern Yellow Sea. Ocean Engineering. 131, 186-196.

[25] Wang, Y.D., Wang, P., Sun, P.F., 2021. A review of autonomous underwater robot control technology. World Science and Technology Research and Development. 43(6), 636.

[26] Feng, Zh.P., 2005. Review of the development status of foreign autonomous underwater robots. Torpedo Technology. (01), 5-9.

[27] Wynn, R.B., Huvenne, V.A.I., Le Bas, T.P., et al., 2014. Autonomous Underwater Vehicles (AUVs): Their past, present and future contributions to the advancement of marine geoscience. Marine Geology. 352, 451-468.

[28] Yu, M.G., Zhang, X., Chen, Z.H., 2017. A review of autonomous underwater robotics. Mechatronics Engineering Technology. 46(08), 155-157.

[29] Alt, C.V., 2003. REMUS 100 Transportable Mine Countermeasure Package. Oceans. IEEE, Proceedings, San Diego, California, USA.

[30] Jaffre, F., Littlefield, R., Grund, M., et al., 2019. Development of a new version of the remus 6000 autonomous underwater vehicle. OCEANS 2019-Marseille. IEEE. pp. 1-7.

[31] Li, D., Ji, D., Liu, J., et al., 2016. A multi-model EKF integrated navigation algorithm for deep water AUV. International Journal of Advanced Robotic Systems. 13(1), 3.

[32] "Wukong" sets a new record for AUV dive depth in China. Sensor World. 2021. 27(04), 31.

[33] Cui, W., 2018. An overview of submersible research and development in China. Journal of Marine Science and Application. 17(4), 459-470.

[34] Cao, X., Sun, H., Jan, G.E., 2018. Multi-AUV cooperative target search and tracking in unknown underwater environment. Ocean Engineering. 150, 1-11.

[35] Kim, K., Tamura, K., 2016. The Zipangu of the Sea project overview: focusing on the R&D for simultaneous deployment and operation of multiple AUVs. Offshore Technology Conference Asia. OnePetro.

[36] Tarwadi, P., Shiraki, Y., Ganoni, O., et al., 2020. Design and Development of a Robotic Vehicle for Shallow-Water Marine Inspections. arXiv preprint arXiv:2007.04563.

[37] Nicolas, T., Vincent, M., Steven, L.B., 2020. Innovative Use of a Rov to Control Underwater Coastal Protections. Offshore Technology Conference. OnePetro.

[38] Xia, P., McSweeney, K., Wen, F., et al., 2022. Virtual Telepresence for the Future of ROV Teleoperations: Opportunities and Challenges. SNAME 27th Off-

shore Symposium. OnePetro.

[39] He, Y., Wang, D.B., Ali, Z.A., 2020. A review of different designs and control models of remotely operated underwater vehicle. Measurement and Control. 53(9-10), 1561-1570.

[40] Aras, M.S.M., Abdullah, S.S., Azis, F.A., 2015. Review on auto-depth control system for an unmanned underwater remotely operated vehicle (ROV) using intelligent controller. Journal of Telecommunication, Electronic and Computer Engineering (JTEC). 7(1), 47-55.

[41] Chen, Z.H., Sheng, Y., Hu, B., 2014. The development status and application of ROV in marine scientific research. Science and Technology Innovation and Application. (21), 3-4.

[42] Xia, Q.S., Liu, Y.H., 2013. Research status and prospect of underwater target fusion identification technology. Torpedo Technology. 21(03), 234-240.

[43] Guan, M., Cheng, Y., Li, Q., et al., 2019. An effective method for submarine buried pipeline detection via multi-sensor data fusion. IEEE Access. 7, 125300-125309.

[44] Rahman, S., 2020. A Multi-Sensor Fusion-Based Underwater Slam System. University of South Carolina.

[45] Xing, H., Liu, Y., Guo, S., et al., 2021. A Multi-Sensor Fusion Self-Localization System of a Miniature Underwater Robot in Structured and GPS-Denied Environments. IEEE Sensors Journal. 21(23), 27136-27146.

[46] Wu, Y., Ta, X., Xiao, R., et al., 2019. Survey of underwater robot positioning navigation. Applied Ocean Research. 90, 101845.

[47] Guleria, K., Atham, S.B., Kumar, A., 2021. Data Fusion in Underwater Wireless Sensor Networks and Open Research Challenges. Energy-Efficient Underwater Wireless Communications and Networking. IGI Global. pp. 67-84.

[48] Balckman, S.S., 1990. Association and fusion of multiple sensor data. Chapter 6: in multitarget-multisensor tracking: advanced applications.

[49] Liu, Y., 2020. Research on multi-sensor-based vehicle environment sensing technology. Changchun University of Science and Technology.

[50] Li, C., Zhu, G., 2019. Underwater multi-sensor Bayesian distributed detection and data fusion. MATEC Web of Conferences. EDP Sciences. 283, 07014.

[51] Shao, Z.Zh., 2013. Multi-sensor data fusion in hydroacoustic signal processing. China Science and Technology Information. (09), 63.

BILINGUAL
PUBLISHING CO.
Pioneer of Global Academics Since 1984

Tel:+65 65881289
E-mail: contact@bilpublishing.com
Website:ojs.bilpublishing.com

ISSN 2661-3247
01
9 772661 324214